



**HAL**  
open science

# Metamorphic Facies and Deformation Fabrics Diagnostic of Subduction: Insights From 2D Numerical Models

Alessandro Regorda, Maria Iole Spalla, Manuel Roda, Jean-Marc Lardeaux,  
Anna Maria Marotta

## ► To cite this version:

Alessandro Regorda, Maria Iole Spalla, Manuel Roda, Jean-Marc Lardeaux, Anna Maria Marotta. Metamorphic Facies and Deformation Fabrics Diagnostic of Subduction: Insights From 2D Numerical Models. *Geochemistry, Geophysics, Geosystems*, 2021, 22 (10), pp.e2021GC009899. 10.1029/2021GC009899 . hal-03451011

**HAL Id: hal-03451011**

**<https://hal.science/hal-03451011>**

Submitted on 26 Nov 2021

**HAL** is a multi-disciplinary open access archive for the deposit and dissemination of scientific research documents, whether they are published or not. The documents may come from teaching and research institutions in France or abroad, or from public or private research centers.

L'archive ouverte pluridisciplinaire **HAL**, est destinée au dépôt et à la diffusion de documents scientifiques de niveau recherche, publiés ou non, émanant des établissements d'enseignement et de recherche français ou étrangers, des laboratoires publics ou privés.




# Geochemistry, Geophysics, Geosystems®



## RESEARCH ARTICLE

10.1029/2021GC009899

## Metamorphic Facies and Deformation Fabrics Diagnostic of Subduction: Insights From 2D Numerical Models

Alessandro Regorda<sup>1</sup> , Maria Iole Spalla<sup>1</sup>, Manuel Roda<sup>1</sup> , Jean-Marc Lardeaux<sup>2,3</sup>, and Anna Maria Marotta<sup>1</sup> 

<sup>1</sup>Dipartimento di Scienze della Terra 'A. Desio', Università degli Studi di Milano, Milano, Italy, <sup>2</sup>Université Nice Sophia-Antipolis, UMR Géozaur, Valbonne, France, <sup>3</sup>Centre for Lithospheric Research, Czech Geological Survey, Prague, Czech Republic

### Key Points:

- The existence of contrasted metamorphic domains broadens the interpretation of thermal states in converging systems, contrasting the perspective that identifies each single metamorphic facies series as representative of a specific geodynamic process
- The varieties of metamorphic gradients recorded during subduction increases with the increment of convergence velocity
- Mylonitic fabrics dominate in high-pressure-LT metamorphic facies in continental crust associated with serpentinized mantle, as observed in highly deformed tectonic mélange described in the internal domains of the Alps

### Correspondence to:

A. Regorda,  
alessandro.regorda@unimi.it

### Citation:

Regorda, A., Spalla, M. I., Roda, M., Lardeaux, J.-M., & Marotta, A. M. (2021). Metamorphic facies and deformation fabrics diagnostic of subduction: Insights from 2D numerical models. *Geochemistry, Geophysics, Geosystems*, 22, e2021GC009899. <https://doi.org/10.1029/2021GC009899>

Received 12 MAY 2021

Accepted 18 SEP 2021

**Abstract** We developed a 2D numerical model that simulates the evolution of a subduction in order to analyze which different metamorphic facies and deformation fabrics can be recorded within a subduction complex and whether the subduction velocity can influence their distribution. Regions with pressure and temperature (P-T) conditions characteristic of different metamorphic facies have been explored in the different domains of the subduction system to verify the existence of associations that may result as diagnostic of specific areas of the subduction system at different times. Distribution patterns of strain rates and relative deformation fabrics have also been investigated to verify whether they can be recorded under different metamorphic facies conditions. Our results show that three domains characterized by contrasting metamorphic conditions can be simultaneously observed in different regions of the subduction complex, in contrast with the widespread idea that different metamorphic series are representative of peculiar geodynamic scenarios, but in agreement with the commonly observed coexistence of contrasted P-T conditions in orogenic belts. In addition, we verified that mylonitic fabrics can develop more frequently in metamorphic facies characterized by high Pressure/Temperature (P/T) ratios, while coronitic fabric can be better preserved in metamorphic facies with low-to-medium P/T ratios.

**Plain Language Summary** The use of numerical modeling in geosciences allow us to better understand the mechanisms involved in geodynamic processes that take place on a large scale. Here we use a numerical simulation of the convergence between tectonic plates in which one plate subducts under the other. We do this in order to analyze pressure and temperature conditions recorded in different portions of subduction systems, and to investigate whether deformations that we observe in rocks depend on particular pressure and temperature conditions. Our results show that areas characterized by high pressures and low temperatures and areas characterized by low pressures and high temperatures can be simultaneously observed in different portions of the subduction system. These results are in contrast with the widespread idea that specific pressure and temperature conditions are peculiar to specific geodynamic processes, such as the oceanic subduction or the continental collision. Ultimately, our research suggests that geodynamic reconstructions deriving from data collected on field might be taken carefully.

## 1. Introduction

Following the pioneering works carried out in the seventies (e.g., England & Richardson, 1977; Oxburgh & Turcotte, 1970, 1971; Toksöz & Bird, 1977) several key advances have been made in numerical modeling methods that have improved the understanding of the thermo-mechanical evolution of the oceanic and continental lithosphere during oceanic subduction and continental collision (e.g., Billen, 2008; Cloos, 1982, 1983, 1993; Cloos & Shreve, 1988a, 1988b; England & Thompson, 1984; Gerya & Stöckhert, 2006; Gerya et al., 2002; Luoni et al., 2020; Magni et al., 2014; Marotta & Spalla, 2007; Peacock, 1989, 1990b; Roda et al., 2011, 2012; Thompson, 1981; van Hunen & Allen, 2011). In particular, several models have shown the importance of dehydration-hydration reactions (e.g., Arcay et al., 2005; Faccenda et al., 2009; Faccenda & Mancktelow, 2010; Guillot et al., 2001; Meda et al., 2010; Peacock, 1990a; Quinquis & Buitert, 2014; Rupke et al., 2004; Wang et al., 2019) on the mantle wedge dynamics, with the activation of short wavelength convective cells consequent to the serpentinization and the associated decrease in viscosity (Gerya et al., 2002;

© 2021. The Authors.

This is an open access article under the terms of the [Creative Commons Attribution-NonCommercial-NoDerivs License](https://creativecommons.org/licenses/by-nc-nd/4.0/), which permits use and distribution in any medium, provided the original work is properly cited, the use is non-commercial and no modifications or adaptations are made.

Hebert et al., 2009; Hirth & Kohlstedt, 2003; Honda & Saito, 2003; Meda et al., 2010; Regorda et al., 2017; Roda et al., 2010).

2D thermo-mechanical models can help to explore both the spatial distribution and temporal evolution, in subduction/collision systems, of fields characterized by P-T conditions corresponding to the different metamorphic facies (Eskola, 1915; 1920; Fettes & Desmond, 2007; Turner, 1981). Traditionally three metamorphic series with different P/T ratios have been identified from petro-structural analysis of orogenic belts, and they are usually associated with different stages of evolution of a convergent margin (e.g., Ernst, 1976, 1977; Kornprobst, 2002; Spear, 1993; Yardley & Warren, 2020):

1. Metamorphic series with high P/T ratios, deduced by regional scale distribution of dominant metamorphic imprints (e.g., Ernst, 1973; Miyashiro, 1961), are generally associated with Pressure-Temperature (P-T) conditions interpreted as peculiar of subduction and are referred to as Franciscan (or Sanbagawa) metamorphic sequences.
2. Barrovian (or Dalradian) metamorphic series, which are characterized by intermediate P/T ratios, are traditionally interpreted as the effect of crustal thickening during continental collision both by mountain belt tectono-metamorphic analyzes and by thermo-mechanical modeling predictions (e.g., Barrow, 1912; Bohlen, 1987; England & Richardson, 1977; England & Thompson, 1984; Jamieson et al., 1998; Sandiford & Powell, 1991; Thompson, 1981; Thompson & England, 1984).
3. Metamorphic facies series characterized by low P/T ratios (Abukuma or Buchan-type metamorphism) have been generally associated with abnormally high geothermal gradients such as those of the island arc or ridge settings (Cloos, 1993; Fagan et al., 2001; Favier et al., 2019; Mevel et al., 1978; Oxburgh & Turcotte, 1970; Verati et al., 2018), slab rollback or increase of the slab dip after continental collision (Ji et al., 2019; Li et al., 2013; Menant et al., 2016; Schliﬀke et al., 2019; Sizova et al., 2019), post-collisional extension (Carmignani & Kligfield, 1990; Vanderhaeghe, 2012), melt migration through the crust (Depine et al., 2008), local effects of contact metamorphism (Rothstein & Manning, 2003).

Miyashiro (1961, 1973) promoted the concept of paired metamorphic belts, revisited by Brown (2010), and based on the juxtaposition along orogenic crustal sections of tectonic complexes characterized by Franciscan- and Abukuma-type metamorphic facies series. In addition, in some orogenic belts, the high-pressure (HP) units show significantly contrasted P-T metamorphic conditions during subduction. For example, in the European Variscan belt, significantly contrasted P-T metamorphic conditions have been recorded by the rocks during the Variscan subduction, from blueschist, to eclogite and HP-granulite facies (e.g., see synthesis and references in Ballèvre et al., 2009; Faure et al., 2005, 2008, 2009; Lardeaux, 2014b; Lardeaux et al., 2014; Regorda et al., 2020). In the Alps, detailed P-T-t paths reconstructions highlight different thermal gradients recorded by specific metamorphic units during their evolution within the Alpine subduction zone (e.g., Berger & Bousquet, 2008; Lardeaux et al., 2014; Roda et al., 2012; Spalla et al., 1996, and references therein). These occurrences suggest that a thermal gradient (or P/T ratio) is not peculiar of a single geodynamic process, but contrasted gradients and thermal states can be recorded in the same geological setting, as a function of the burial and exhumation paths of tectonic slices involved in a subduction/collision system.

Moreover, thermo-mechanical numerical models can help to quantify strain rates and relate them to different regions of the subduction/collision complex (Beach, 1976; Gosso et al., 2015; Lardeaux et al., 1982; Lardeaux & Spalla, 1990; Passchier & Trouw, 2005; Pognante et al., 1985; Ramsay & Graham, 1970; Spalla & Zucali, 2004; Spry, 1969; Teall, 1885). However, since the development of different fabrics is strongly influenced by many other factors, such as the temperature, grain size and the mineral rock composition (e.g., Handy et al., 1999; Passchier & Trouw, 2005), we analyzed the strain rates field in different structural level in the crust and in different parts of the subduction complex to verify if coronitic, tectonic or mylonitic fabrics could develop with higher probabilities under particular P-T conditions. Many authors (e.g., Fry, 1979; Herwegh et al., 1997; Mehl & Hirth, 2008; Norris & Cooper, 2003; Okudaira & Shigematsu, 2012; Piffner & Ramsay, 1982; Prior et al., 1990; White, 1979) have correlated the deformation observed in the rocks with strain rate and the finite strain accumulated. Strain rates between  $10^{-15} \text{ s}^{-1}$  and  $10^{-13} \text{ s}^{-1}$  are necessary to produce regional scale structures in orogenic belts (Piffner & Ramsay, 1982), while narrow localized shear zones can be easily developed in case of strain rates higher than  $10^{-13} \text{ s}^{-1}$  (Mehl & Hirth, 2008; Okudaira & Shigematsu, 2012). Mylonites are usually associated with very high strain rates ( $10^{-12} \text{ s}^{-1}$  to  $10^{-10} \text{ s}^{-1}$ ) over

very short time periods (500–50,000 years, Pfiffner & Ramsay, 1982; Prior et al., 1990) or with lower strain rates (in the order of  $10^{-13} \text{ s}^{-1}$ ) over time periods up to 5 Ma (Pfiffner & Ramsay, 1982). Differently, coronites can be preserved for strain rates lower than  $10^{-15} \text{ s}^{-1}$  (Pfiffner & Ramsay, 1982). These thresholds are considered effective for different rock types and therefore we use them as reference to evaluate the probability to develop coronitic, tectonic and mylonitic textures, both in the continental and in the oceanic crust. In the Alps, rocks deeply involved in the subduction complex and recording P-T conditions compatible with blueschist and eclogite metamorphic facies can be observed in the axial zone of the chain, and generally show heterogeneous deformation with dominant tectonic or mylonitic fabrics (e.g., Gasco et al., 2011; Lardeaux, 2014a; Malatesta et al., 2012; Oberhänsli & Goffé, 2004; Roda et al., 2021; Zucali et al., 2020). These rocks are often associated with serpentinites (e.g., Assanelli et al., 2020; Gasco et al., 2011; Lardeaux, 2014a; Malatesta et al., 2012; Manzotti et al., 2014; Roda et al., 2020), which have a crucial role in exhumation mechanisms (Gerya et al., 2002; Guillot et al., 2009; Luoni et al., 2020; Meda et al., 2010; Roda et al., 2012; Schwartz et al., 2001; Tamblyn et al., 2020; Warren et al., 2008; Yamato et al., 2007). Differently, Alpine HP metamorphism has not been recorded by rocks from the external domains of the Alps, which generally show a lower amount of finite deformation under P-T conditions compatible with zeolite, prehnite-pumpellyite, greenschist and epidote-amphibolite metamorphic facies (e.g., Handy & Oberhänsli, 2004; Lardeaux, 2014a).

The aim of this work is to analyze where different metamorphic facies and deformation fabrics can develop within a subduction complex and to evaluate the influence of the subduction velocity on their distribution. We considered subduction velocities of 3, 5, and 8  $\text{cm yr}^{-1}$  to simulate the evolution of slow, intermediate and fast subduction systems, respectively. Velocities of 3 and 8  $\text{cm yr}^{-1}$  have been chosen to describe slower and faster subduction zones (observed respectively in portions of Central and in South America and the Philippines; e.g., Cruciani et al., 2005; Lallemand et al., 2005), respectively. The velocity of 5  $\text{cm yr}^{-1}$  has been chosen to represent a moderate velocity convergence system, in accordance with the subduction velocities generally accepted for the Variscan convergence (Regorda et al., 2020, and refs. therein). Although many other parameters, such as the age of the subducted slab and the slab dip, can have an impact on both the thermal field and the geodynamic evolution of the subduction system, previous works have shown the crucial role of the subduction velocity (e.g. Arcay et al., 2005; Hebert et al., 2009; Regorda et al., 2017, 2020). Consequently, here we decided to focus our study only on the impact of the subduction velocity, considering the geometry of an average subduction system. The results predicted by the models have been analyzed in terms of strain rates and metamorphic facies developed only on crustal rocks, highlighting their position in the subduction complex.

## 2. Model Setup

We developed three models characterized by different subduction velocities to reproduce the thermo-mechanical evolution of a subduction, whose duration depends on the time needed to subduct a 2,500 km-wide ocean. The physics is described by the equations of continuity, of conservation of momentum and of conservation of energy (e.g., Thieulot, 2014; Tosi et al., 2015; van Keken et al., 1997, 2008), which can be expressed as follows:

$$\frac{\partial \rho}{\partial t} + \nabla \cdot (\rho \mathbf{u}) = 0 \quad (1)$$

$$-\nabla p + \nabla \cdot \boldsymbol{\tau} + \rho \mathbf{g} = 0 \quad (2)$$

$$\rho C_p \left( \frac{\partial T}{\partial t} + \mathbf{u} \cdot \nabla T \right) = \nabla \cdot (k \nabla T) + H_r + H_s + H_a \quad (3)$$

where  $\mathbf{u}$  is the velocity,  $p$  is the pressure,  $\boldsymbol{\tau}$  is the deviatoric stress,  $\rho$  is the density,  $\mathbf{g}$  is the gravity acceleration,  $C_p$  is the heat capacity at constant pressure,  $T$  is the temperature,  $k$  is the thermal conductivity,  $H_r$  is the radiogenic heating per mass unit,  $H_s = \tau_{ij} \dot{\epsilon}_{ij}$  is the shear heating and  $H_a = T \alpha \frac{Dp}{Dt}$  is the adiabatic heating, where  $\alpha$  is the thermal expansion coefficient. Density variations due to temperature are generally small enough to assume the density as constant ( $\rho = \rho_0$ ) in Equation 1 and in Equation 3, while it must be treated as a variable in the buoyancy term of Equation 2, such that

**Table 1**

Values of the Material and Rheological Parameters Used in the Analysis.  $\eta_0$  and  $\rho_0$  Are the Reference Viscosity and Density for Each Material, Respectively

	Continental crust	Upper oceanic crust	Lower oceanic crust	Dry mantle	Serpentinized mantle
Rheology	Dry granite	-	Diabase	Dry dunite	-
$E$ (kJ mol <sup>-1</sup> )	123	-	260	444	-
$n$	3.2	-	2.4	3.41	-
$\eta_0$ (Pa s)	$3.47 \times 10^{21}$	$10^{19}$	$1.61 \times 10^{22}$	$5.01 \times 10^{20}$	$10^{19}$
$\rho_0$ (kg/m <sup>3</sup> )	2,640	2,961	2,961	3,200	3,000
$K$ (W/mK)	3.03	2.10	2.10	4.15	4.15
$H_r$ ( $\mu$ W m <sup>-3</sup> )	2.5	0.4	0.4	0.002	0.002
References	a,d,f	b,f,i,j,k	a,b,c,f	c,d,e,f,j	d,f,g,h,i

<sup>a</sup>Ranalli and Murphy (1987). <sup>b</sup>Afonso and Ranalli (2004). <sup>c</sup>Kirby (1983). <sup>d</sup>Haenel et al. (1988). <sup>e</sup>Chopra and Peterson (1981). <sup>f</sup>Dubois and Diamant (1997) and Best and Christiansen (2001). <sup>g</sup>Roda et al. (2011). <sup>h</sup>Schmidt and Poli (1998). <sup>i</sup>Gerya and Stöckhert (2006). <sup>j</sup>Roda et al. (2012). <sup>k</sup>Gerya and Yuen (2003).

$$\rho = \rho_0(1 - \alpha(T - T_0))$$

where  $\rho_0$  is the density at a reference temperature  $T_0$ . Equation 1 then can be rewritten as

$$\nabla \cdot \mathbf{u} = 0 \quad (4)$$

This simplification is known as the extended Boussinesq approximation (e.g., Christensen & Yuen, 1985; Gerya, 2010; Ismail-Zadeh & Tackley, 2010). The equation of conservation of momentum has been integrated using the penalty function formulation, while the Petrov-Galerkin method has been used to integrate the equation of conservation of energy. Numerical integration has been performed by means of the 2D finite elements code SubMar (Marotta et al., 2006), in a rectangular domain 1,400 km wide and 700 km deep, discretized by a non-deforming irregular grid composed by quadratic triangular elements, carrying a denser nodal distribution near the contact region between the plates, where the most significant gradients in temperature and velocity fields are expected. The horizontal and vertical sizes of the elements vary from 30 to 2.5 km, with the smallest elements located in proximity to the active margin region to a depth of 300 km. Four hundred fifty-five thousand four hundred eighty-nine markers with different indexes are distributed in the domain with a density of one marker per 0.25 km<sup>2</sup>, to compositionally differentiate the characteristic lithologic composition of lower and upper continental and oceanic crust, and lithospheric mantle of the upper plate, while no markers have been introduced in the asthenospheric mantle. Rock properties and rheological parameters are listed in Table 1.

The model combines a linear viscous rheology for the sublithospheric mantle with a linear viscoplastic rheology for the lithosphere. For each material  $i$ , the viscous component is calculated as

$$\mu_i^{visc} = \mu_{0i} e^{\frac{Ea_i}{R} \left( \frac{1}{T} - \frac{1}{T_0} \right)} \quad (5)$$

where  $T$  is the temperature and  $\mu_{0i}$  and  $Ea_i$  are the reference viscosity and the activation energy at the reference temperature  $T_0$ , respectively. The plastic component  $\mu_i^{plast}$  is computed combining the Byerlee's law and the Tresca criterion (Regorda et al., 2017). In the lithospheric layer the effective viscosity is defined as

$$\mu_i^{eff} = \min \left[ \mu_i^{plast}, \mu_i^{visc} \right] \quad (6)$$

The rheological weakening of the mantle wedge has been simulated by assuming a constant viscosity of  $10^{19}$  Pa s for the serpentinized mantle (Arcay et al., 2005; Gerya & Stöckhert, 2006; Honda & Saito, 2003; Roda et al., 2010). The stability field of serpentine (Schmidt & Poli, 1998) has been delimited inside the hydrated mantle wedge, which is limited from below by the subducting plate (see details in Marotta et al., 2020; Regorda et al., 2017, 2020). With respect to the original SubMar of Marotta et al. (2006), the code has been implemented taking into account mantle hydration, phase transitions and latent heat, as described in detail in Marotta et al. (2020), while partial melting has not been taken into account.

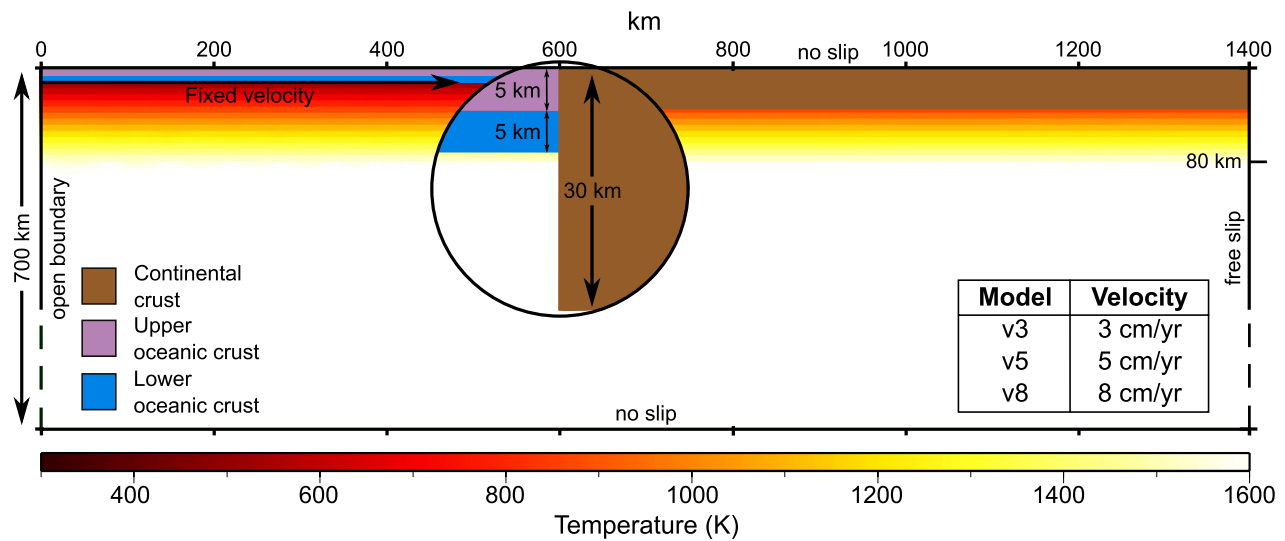


**Figure 1.** Model geometry showing layer thicknesses and the initial temperature profile.

Since metamorphic facies characterized by HT and LP can develop in the superficial layers of the continental crust as consequence of partial melting and melt migration (e.g., Depine et al., 2008), the absence of these mechanisms could be a limitation, preventing the development of specific metamorphic conditions. Similarly, since our code does not account for strain localization, the models could not be able to predict the development of highly localized zones that can experience very high strain rates ( $>10^{-11} \text{ s}^{-1}$ ), as suggested by experimental analysis (e.g., Okudaira & Shigematsu, 2012).

Dirichlet or Neumann boundary conditions for velocities and temperatures are used along different boundaries of the 2D domain. The velocity boundary conditions correspond to no-slip conditions along the upper and the lower boundaries of the 2D domain and free-slip conditions along the right boundary, while the left boundary is open, in order to allow inflow and outflow of material. In addition, a velocity of 3, 5, or 8  $\text{cm yr}^{-1}$  (hereinafter referred as models v3, v5, and v8, respectively) is prescribed along the bottom of the oceanic crust to drive the closure of the 2,500 km-wide ocean in 85, 51, and 32 Ma, respectively. The same velocity is also fixed along a 45 dipping plane that extends from the trench to a depth of 100 km to facilitate the trigger of the subduction.

The thermal boundary conditions correspond to fixed temperatures at the top ( $27^\circ\text{C}$ ) and the bottom ( $1327^\circ\text{C}$ ) of the model, zero thermal flux at the right vertical sidewall and fixed temperature along the left side of the model where temperature remains unchanged from the initial values. The initial thermal structure corresponds to a simple conductive thermal configuration throughout the lithosphere, with temperatures that vary from  $27^\circ\text{C}$  at the surface to  $1327^\circ\text{C}$  at its base, and a constant temperature of  $1327^\circ\text{C}$  below the lithosphere. The base of the lithosphere is located at a depth of 80 km under both the oceanic and continental plates. This configuration corresponds to both an oceanic lithosphere of approximately 40 Ma, based on the cooling of a semi-infinite half space model (Turcotte & Schubert, 2002), and a thinned continental passive margin based on a medium to slow spreading rate of 2–3  $\text{cm yr}^{-1}$  during continental rifting (e.g., Marotta et al., 2016). The  $1327^\circ\text{C}$  isotherm defines the base of the lithosphere throughout the evolution of the system. The initial geometry of the model is synthesized in Figure 1.

The P-T distribution of metamorphic facies has been here synthesized from different authors (Ernst & Liou, 2008; Spear, 1993; Yardley, 1989) and summarized in Figure 2, where their boundaries have been necessarily discretized, mediating the diffuse limits proposed by the various authors, for their integration in the performed models. Greenschist, zeolite and prehnite-pumpellyite limits are in agreement with Spear (1993) and they correspond to greenschist and sub-greenschist facies of other authors (e.g., Bousquet et al., 2008; Ernst, 2001; Fettes & Desmond, 2007).



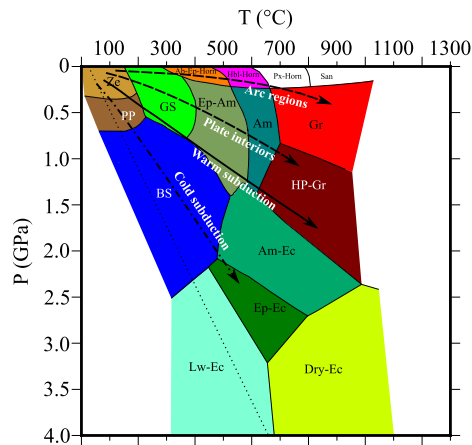


**Figure 2.** Petrogenetic P-T grid for crustal rocks used in our models (modified after Ernst & Liou, 2008; Spear, 1993; Yardley, 1989). Black arrows represent geothermal gradients traditionally associated to arc regions and collision zones (dashed arrows), warm subduction complexes (continuous arrow) and cold subduction complexes (dashed-dotted arrow), as presented by Cloos (1993). Black dotted lines represent very low subduction-zone geothermal gradient ( $5^{\circ}\text{C km}^{-1}$ ). Metamorphic facies abbreviations: Ab-Ep-Horn, albite-epidote hornfels; Am, amphibolite; Am-Ec, amphibole-eclogite; BS, blueschist; Dry-Ec, dry eclogite; Ep-Am, epidote amphibolite; EC, eclogite; Ep-Ec, epidote-eclogite; Gr, granulite; GS, greenschist; Hbl-Horn, hornblende hornfels; HP-Gr, high pressure-granulite; Lw-Ec, lawsonite-eclogite; PP, prehnite-pumpellyite; Px-Horn, pyroxene hornfels; San, Sanidinite; Ze, Zeolite.

### 3. Model Results

Below, we will describe the numerical results focusing on: (a) the thermal evolution of the models; (b) the spatial distribution of metamorphic facies inside the subduction complex at different times; (c) the strain rates possibly recordable by rock volumes deforming under different metamorphic environment (=facies); and (d) the potential distribution of rock fabrics (coronitic, tectonic, and mylonitic) inside the subduction complex.

Fabric development not only depends on the strain rate and the time span over which it operates, but also on many other factors, such as the temperature at which deformation is imposed and the composition of rocks (Handy et al., 1999; Passchier & Trouw, 2005). Consequently, we consider fields defined by specific strain rates just as domains in which different fabrics can be developed with higher probabilities, without taking into account differences in the protolith and in the mineralogy of the rocks. In particular, we consider fields characterized by strain rates higher than  $10^{-13} \text{ s}^{-1}$  as potentially mylonitic, and fields with strain rates lower than  $10^{-15} \text{ s}^{-1}$  as potentially coronitic (Pfiffner & Ramsay, 1982). In the same way, we consider fields where the strain rates are between  $10^{-15} \text{ s}^{-1}$  and  $10^{-13} \text{ s}^{-1}$  as dominantly tectonic, without excluding the possibility to have fabric heterogeneity due to different composition of rocks manifesting coronitic and/or mylonitic textures, spatially subordinated.

#### 3.1. Thermal Evolution

The geodynamic evolution of subduction systems has been thoroughly analyzed and described by many authors (e.g., Arcay et al., 2005; Dai et al., 2018; Gerya, 2011; Gerya & Stöckhert, 2006; Marotta & Spalla, 2007;

Regorda et al., 2017; Roda et al., 2012; Stern & Gerya, 2018; Wang et al., 2019). Here, we will describe only the main features of the thermal evolution of the different models, to highlight the impact of the subduction velocity on the predicted P-T conditions in different parts of the subduction system. Model results show that:

1. The increase in the subduction velocity results in a decrease in the temperatures inside the slab, enlightened by the lower depths reached by isotherms 500 and  $700^{\circ}\text{C}$  in model v3 (Figure 3, panel a) with respect to model v5 (Figure 3, panel b) and, more clearly, to model v8 (Figure 3, panel c). In addition, in models v3 there is a continuous warming of the subducted slab during the evolution (see the distribution of the isotherms in Figure 3, panel a), while model v8 shows a continuous cooling (see the distribution of the isotherms in Figure 3, panel c). For model v5 the subducted slab remains colder than model v3 until approximately 25 Ma of evolution, while afterward it slowly warms up (see isotherm  $700^{\circ}\text{C}$  in Figure 3, panel b).
2. Models v3 and v5 show lower temperatures at the bottom of the upper plate and in the external portion of the mantle wedge with respect to model v8, which is clear observing the shape and the depth of the isotherms 500 and  $700^{\circ}\text{C}$  in Figure 3. In particular, models v3 and v5 show a continuous cooling in the wedge area (see isotherms in Figure 3, panels a and b), while model v8 shows an initial slight cooling followed by an intense warming (see isotherms in Figure 3, panel c).

#### 3.2. Metamorphic Facies

##### 3.2.1. Model v3

The model does not predict P-T conditions compatible with metamorphic facies characterized by low-pressure (LP) and medium- (MT) to high-temperature (HT) conditions, such as granulite and hornfels (Figure 4, panel a). Amphibolite facies conditions are attained only during the first part of the evolution (Figure 4, panel a), at the base of the upper plate crust (Figure 5, panel a1), and it disappears with the progressive

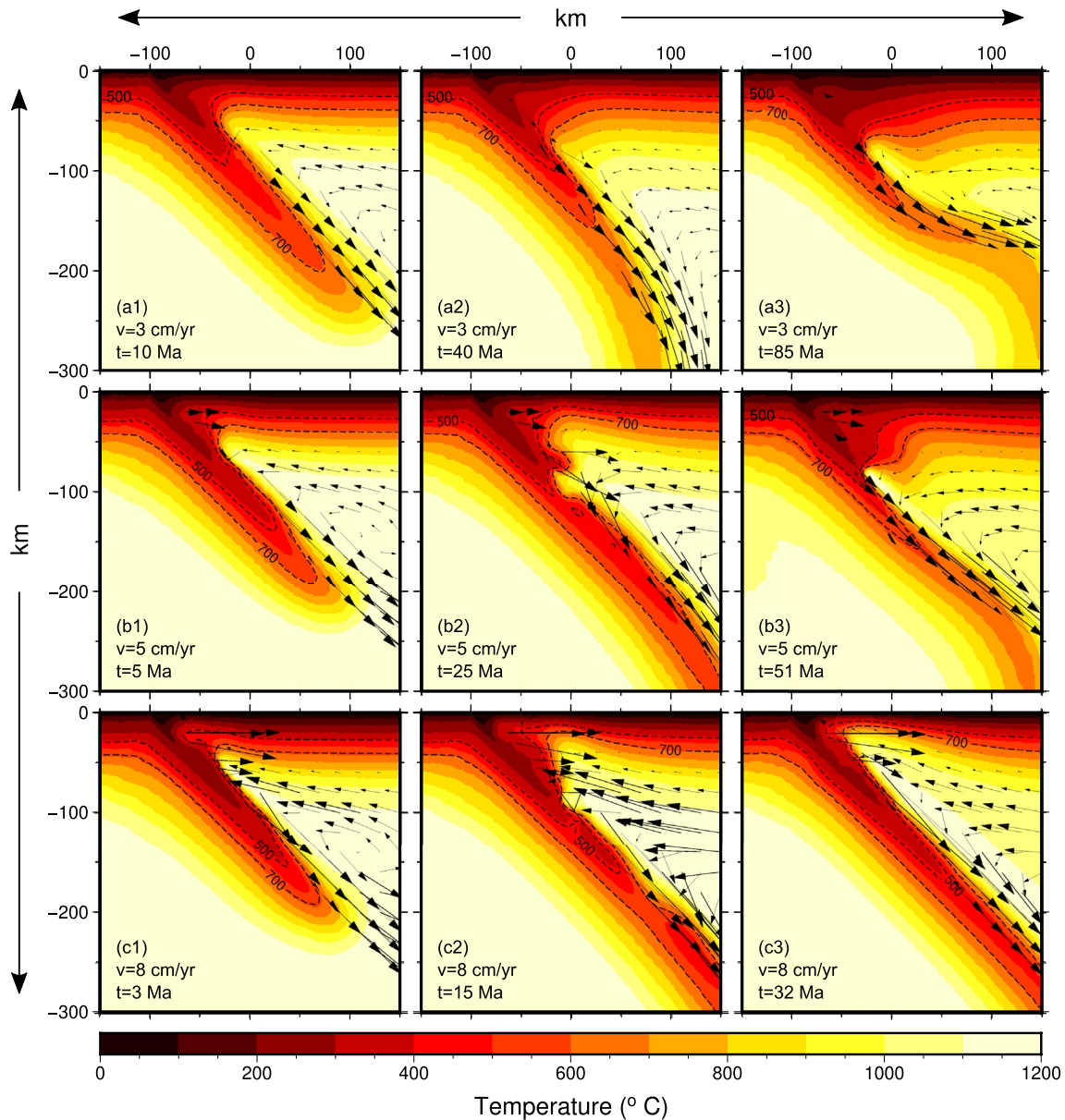


**Figure 3.** Thermal evolution of models v3 (panel a), v5 (panel b) and v8 (panel c). The first column (panels a1–c1) shows the thermal state when the slab has reached 200 km depth, at 10, 5, and 3 Ma of evolution for models v3, v5, and v8, respectively; the second column (panels a2–c2) represents the thermal state at about half of the evolution, at 40, 25, and 15 Ma for models v3, v5, and v8, respectively; and the third column (panels a3–c3) represents the thermal state at the end of the evolution at 85, 51, and 32 Ma for models v3, v5, and v8, respectively. Black arrows represent the velocities of the mantle flow above the slab. Black dashed lines represent isotherms 500 and 700°C.

decrease in temperature. In the same way, the extent of the epidote-amphibolite facies decreases in time (Figure 4, panel a) as temperature decreases always at the base of the upper plate crust (Figure 5, panels a2 and a3). Differently, P-T conditions compatible with the zeolite and greenschist facies are persistently stable in the upper crust of the upper plate (Figure 5, panel a) and the region undergoing greenschist facies conditions enlarges at the expense of the epidote-amphibolite facies over the time (Figure 5, panel a3). The prehnite-pumpellyite facies is stable with continuity in a small portion of the upper crust of the upper plate, close to the trench (Figure 5, panel a).

Blueschist facies conditions are continuously stable during the subduction (Figure 4, panel a), especially in the inner portion of the mantle wedge, close to the slab (Figure 5, panel a), and its extension increases



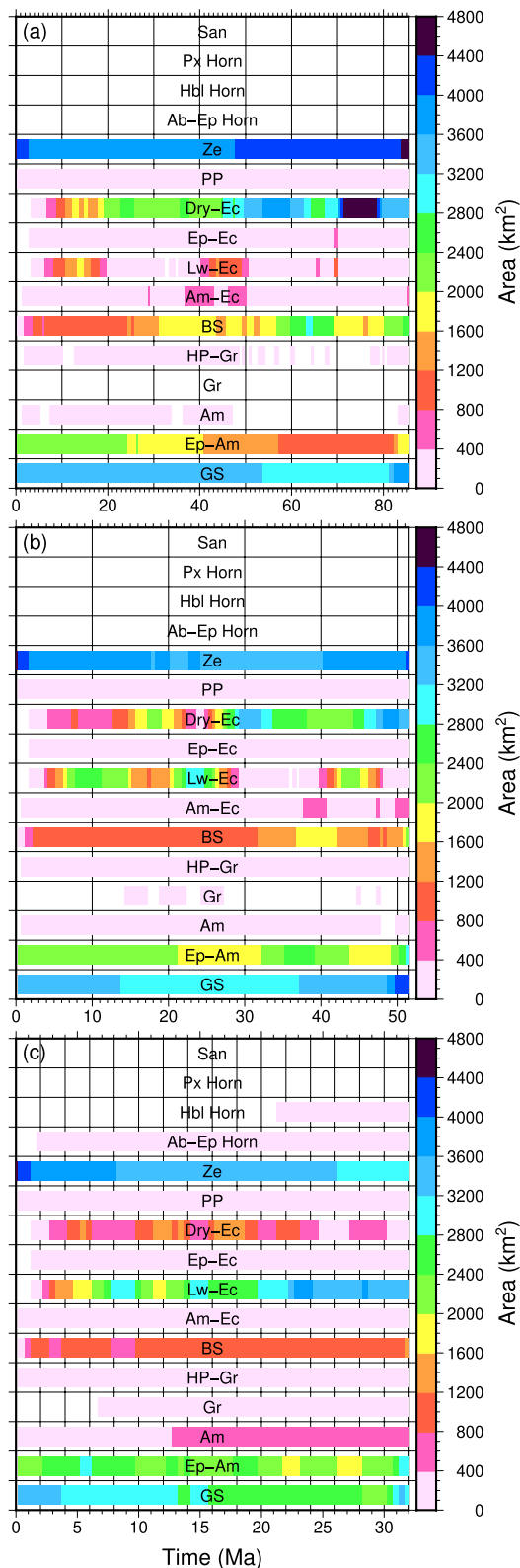


**Figure 4.** Amount of crustal rocks determined for each metamorphic facies during the evolution for model v3 (panel a), model v5 (panel b), and model v8 (panel c). Metamorphic facies abbreviations as in Figure 2.

during the mature stages of the evolution (Figure 4, panel a), when temperatures lower than 500°C are predicted up to approximately 90 km far from the trench (Figure 5, panel a3). The decrease in temperature in the external portion of the wedge determines a larger region undergoing amphibole-eclogite facies conditions during the mature stages of the evolution (Figure 5, panel a). A similar behavior can be observed for the regions affected by epidote-eclogite facies conditions at higher depths, although with a very limited extension (Figure 4, panel a and Figure 5, panel a). Differently, the progressive decrease in temperature in the external portion of the wedge at the end of the evolution results in the disappearance of HP-granulite facies conditions (Figure 4, panel a).

Below approximately 80–90 km of depth, lawsonite-eclogite and dry-eclogite facies conditions are attained and the limit between the two strongly depends on the temperature. Both facies are stable at the beginning of the subduction: the lawsonite-eclogite facies conditions are satisfied in the internal part of the slab, where there are temperatures below 650°C, while the dry-eclogite facies conditions characterize the external portion (Figure 5, panel a1). The temperature increase in the slab results in the progressive disappearance of the lawsonite-eclogite facies regions during the mature stages of evolution (Figure 5, panel a2).

### 3.2.2. Effects of the Subduction Velocity

The increase in the subduction velocity determines the appearance of regions undergoing granulite and hornfels facies conditions, even if in small areas. In particular, granulite facies conditions are attained with discontinuity in model v5 (Figure 4, panel b), while model v8 shows a more continuous occurrence of granulite, hornblende hornfels and albite-epidote hornfels facies (Figure 4, panel c). These metamorphic facies characterize the bottom of the upper plate crust and the shallow and external portion of the wedge during the mature stages of the evolution (Figure 5, panels b2, c2, and c3), as a consequence of the temperature increase for higher velocities. In the same way, the higher temperatures in the upper plate predicted by models v5 and v8 allow that amphibolite facies conditions are achieved during the whole evolution (Figure 4, panels b and c). In particular, model v8 shows the attainment of amphibolite facies conditions in a wide zone at the bottom of the upper plate crust, up to 150 km from the trench (Figure 5, panels c2 and c3). Similarly, the increase of temperature in the upper plate during late evolution in models v5 and v8 results in an increase of the area under epidote-amphibolite facies conditions (Figure 5, panels b3 and c3). However, the increase in temperature of the upper plate results in a reduction of the region characterized by zeolite and greenschist facies conditions (Figure 4 panels b and c), in relation to the contemporary increase of the area affected by epidote-amphibolite facies conditions in the upper plate (Figure 5, panels b and c). The increase in the subduction velocity determines also the extent of portions affected by blueschist facies conditions during the mature evolution, in particular for model v8 (Figure 4, panel c). This is consequent to the intense warming of the external portion of the mantle wedge induced by the large-scale mantle flow underneath the overriding plate, which determines the decrease of the regions with temperatures lower than 500°C (Figure 5, panels b and c). The reduction of area under blueschist facies conditions is counterpoised by the occurrence of HP-granulite facies conditions during the whole evolution (Figure 4, panels b and c and Figure 5, panels b and c), as a consequence of the higher temperatures predicted by

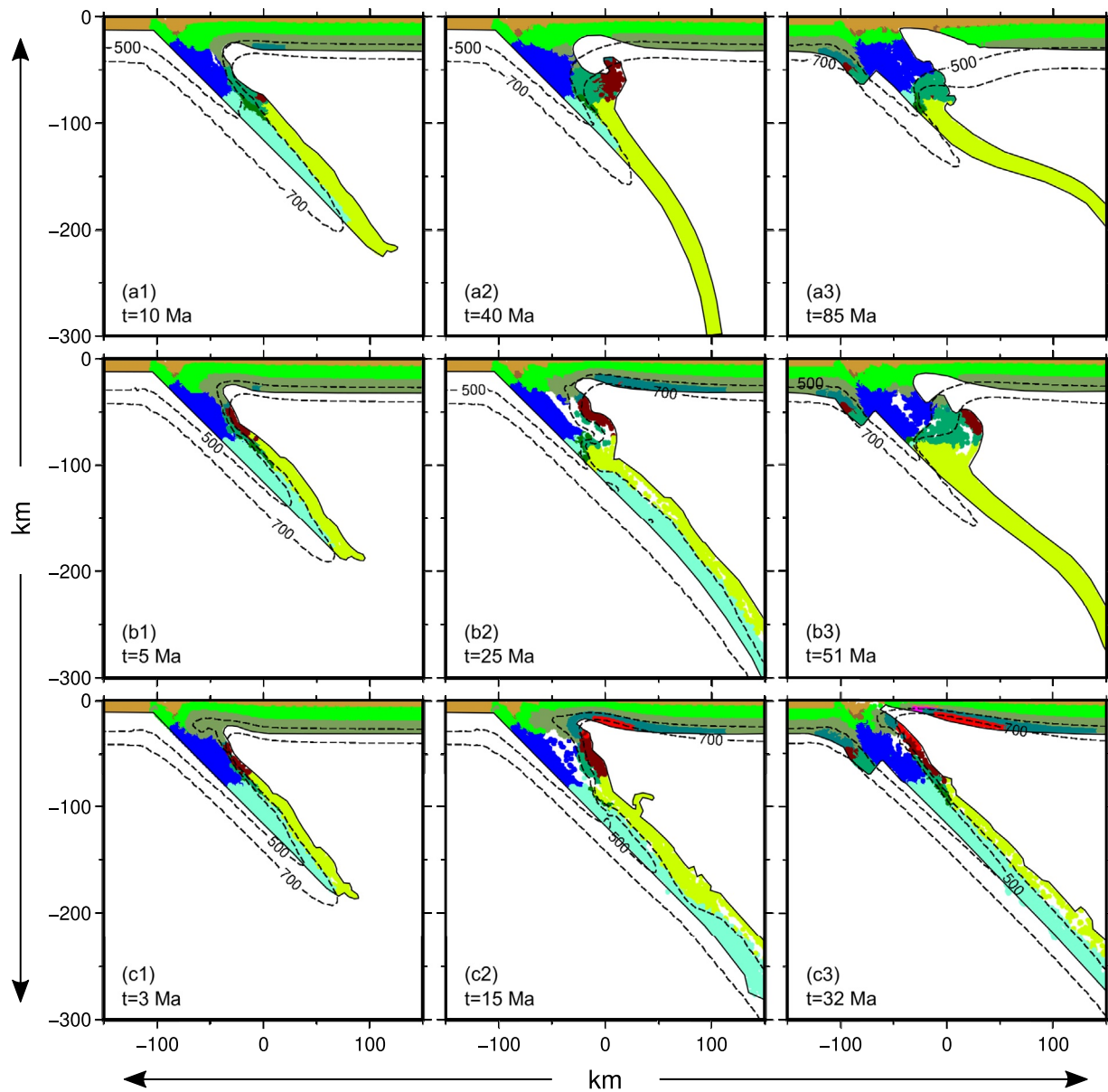


**Figure 5.** Areal distribution in the subduction complex of the metamorphic facies for models v3 (panel a), v5 (panel b), and v8 (panel c). The first column (panels a1–c1) shows the facies distribution when the slab has reached 200 km depth, at 10, 5, and 3 Ma of evolution for models v3, v5, and v8, respectively; the second column (panels a2–c2) represents the facies distribution at about half of the evolution, at 40, 25 and 15 Ma for models v3, v5, and v8, respectively; and the third column (panels a3–c3) represents the facies distribution at the end of the evolution at 85, 51, and 32 Ma for models v3, v5, and v8, respectively. Black continuous lines represent the lower limit of the crust of the upper plate and of the oceanic crust. Black dashed lines represent isotherms 500 and 700°C. Colors of the metamorphic facies as in Figure 2.

models v5 and v8 with respect to model v3. However, model v5 predicts lower temperatures than model v8 in the external portion of the mantle wedge, and this results in the individuation of a region characterized by amphibole-eclogite and epidote-eclogite facies conditions in model v5 comparable to that of model v3 and larger than that of model v8 (Figure 4, panel b with respect to panels a and c, respectively).

Below approximately 80–90 km depth, the existence of lawsonite-eclogite and dry-eclogite metamorphic facies during mature stages of the evolution is strongly influenced by the subduction velocity. Model v5 shows a cold slab during the first half of the evolution, with the consequent co-existence of both lawsonite-eclogite and dry-eclogite facies conditions (Figure 5, panel b2). Differently, the warming predicted during the second half of the evolution determines P-T conditions compatible only with dry-eclogite facies (Figure 5, panel

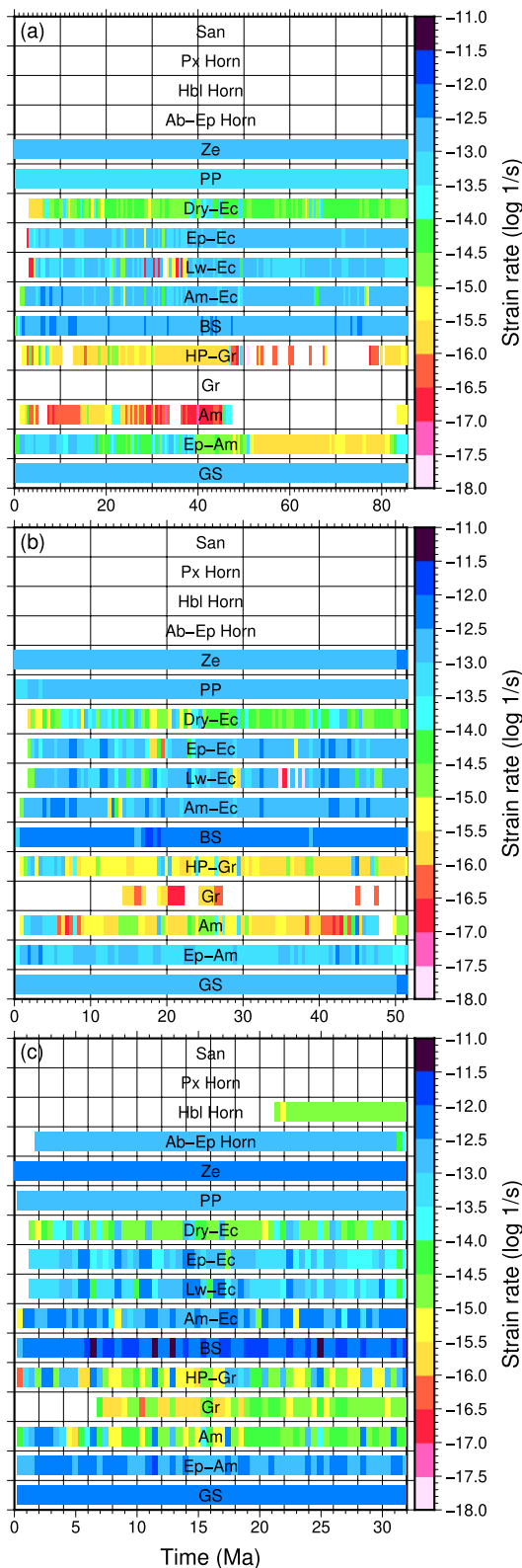


**Figure 6.** Maximum value of strain rates recorded by each metamorphic facies for each time step for model v3 (panel a), model v5 (panel b), and model v8 (panel c). Metamorphic facies abbreviations as in Figure 2.

b3), as observed for model v3. On the contrary, the continuous decrease in temperature that characterized the slab of the high velocity model (v8) allows the occurrence of the lawsonite-eclogite facies conditions until the end of the subduction, in the internal portion of the slab, and the dry-eclogite facies in the external portion (Figure 5, panels b3 and c3).

### 3.3. Strain Rates

For each time step we considered the maximum value of the effective strain rate predicted in each field characterized by different metamorphic facies conditions (Figure 6), in order to verify if tectonic and/or mylonitic fabrics can be expected. Successively, we calculated the potential rock percentages (expressed by the number of the Lagrangian markers) that can record strain rates lower than  $10^{-15} \text{ s}^{-1}$  (green in Figures 7–9), between  $10^{-15} \text{ s}^{-1}$  and  $10^{-13} \text{ s}^{-1}$  (yellow in Figures 7–9) and higher than  $10^{-13} \text{ s}^{-1}$  (red in Figures 7–9), with respect to the total crustal amount undergoing each different metamorphic facies conditions.

#### 3.3.1. Model v3

Regions characterized by metamorphic facies with a low P/T ratio, such as amphibolite and HP-granulite facies, are characterized by maximum strain rates that only occasionally exceed  $10^{-15} \text{ s}^{-1}$  (Figure 6, panel a), indicating a low probability to develop tectonic and mylonitic fabrics. In fact, the crust percentage under amphibolite and HP-granulite facies conditions that can preserve coronitic texture is always close to 100% (green in Figure 7), with the exceptions of few time steps, when a tectonic fabric can be expected (yellow in Figure 7). Slightly higher maximum strain rates can be observed under dry-eclogite facies conditions, where they are mainly between  $10^{-15} \text{ s}^{-1}$  and  $10^{-13} \text{ s}^{-1}$  during the entire evolution (Figure 6, panel a). However, only a maximum of 25% of crust develops a tectonic fabric (yellow in Figure 7), while the largest part still preserves a coronitic texture (green in Figure 7). Similarly, maximum strain rates between  $10^{-15} \text{ s}^{-1}$  and  $10^{-13} \text{ s}^{-1}$  (with occasional peaks above  $10^{-13} \text{ s}^{-1}$ ) is observed during the first half of evolution in crust undergoing epidote-amphibolite facies conditions, while there is a decrease during the mature stages of evolution, mainly below  $10^{-15} \text{ s}^{-1}$  (Figure 6, panel a). Actually, although the largest amount of crustal rocks still preserves a coronitic texture (mostly over 85%; green in Figure 7), during the first half of the evolution tectonic and, occasionally, mylonitic fabric (yellow and red, respectively, in Figure 7) are expected. Model v3 shows maximum strain rates above  $10^{-13} \text{ s}^{-1}$  during the entire evolution under zeolite and greenschist facies conditions (Figure 6, panel a). However, the amount of crust that develops a mylonitic fabric is lower than 5% (red in Figure 7), while a tectonic fabric occurs in approximately 45% of the crust (yellow in Figure 7). Therefore, the largest amount of crustal rocks undergoing these metamorphic facies (green in Figure 7) can preserve a coronitic texture. Differently, in the prehnite-pumpellyite facies the maximum strain rates are always lower than  $10^{-13} \text{ s}^{-1}$  (Figure 6, panel a), but a tectonic fabric develops in more than 70% of the crustal rocks undergoing this metamorphic facies (yellow in Figure 7).

Highest peaks of maximum strain rates (between  $10^{-13} \text{ s}^{-1}$  and  $10^{-12} \text{ s}^{-1}$ ) is observed in crustal portions undergoing blueschist facies conditions (Figure 6, panel a). Here, there is a clear increase of regions that develops mylonitic fabrics (up to 35%; red in Figure 7), and the coronitic texture is

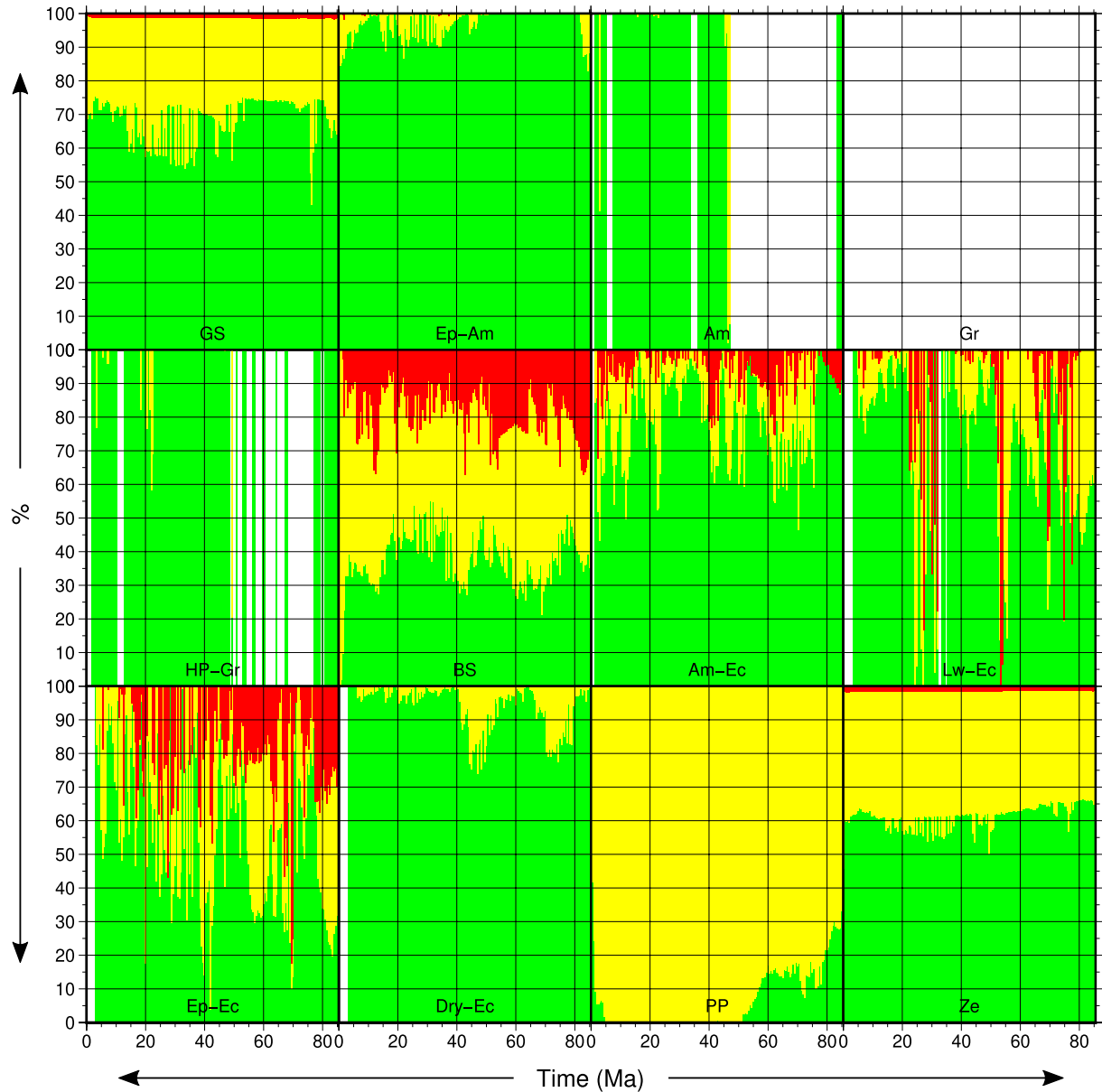


**Figure 7.** Percentages of crustal rocks of model v3 that can record strain rates lower than  $10^{-15} \text{ s}^{-1}$  (green), between  $10^{-15} \text{ s}^{-1}$  and  $10^{-13} \text{ s}^{-1}$  (yellow) and higher than  $10^{-13} \text{ s}^{-1}$  (red) with respect to the total amount of crustal rocks of each metamorphic facies as function of time. White portions indicate the non-existence of the metamorphic facies.

preserved in less than 50% of these parts (green in Figure 7). Under amphibole-eclogite and epidote-eclogite facies conditions maximum attained strain rates are always around  $10^{-13} \text{ s}^{-1}$  (Figure 6, panel a), but in the epidote-eclogite a larger crustal amount develops tectonic and mylonitic fabrics. In fact, the majority of crust undergoing amphibole-eclogite facies conditions preserves a coronitic texture (from 50% to 95%, green in Figure 7) and the mylonitic fabric is expected at maximum in 30% of these rocks (red in Figure 7). Differently, the coronitic domains under the epidote-eclogite conditions vary from 5% to 95% (green in Figure 7) and the mylonitic domains extends up to 80% (red in Figure 7). Maximum strain rates under the lawsonite-eclogite facies conditions are very variable in time, from  $10^{-17} \text{ s}^{-1}$  to  $10^{-13} \text{ s}^{-1}$  (Figure 6, panel a), with repercussion on the extent of different fabric domains. In fact, time spans characterized only by coronitic domains (green in Figure 7) alternate with time spans during which there are only mylonitic domains (red in Figure 7).

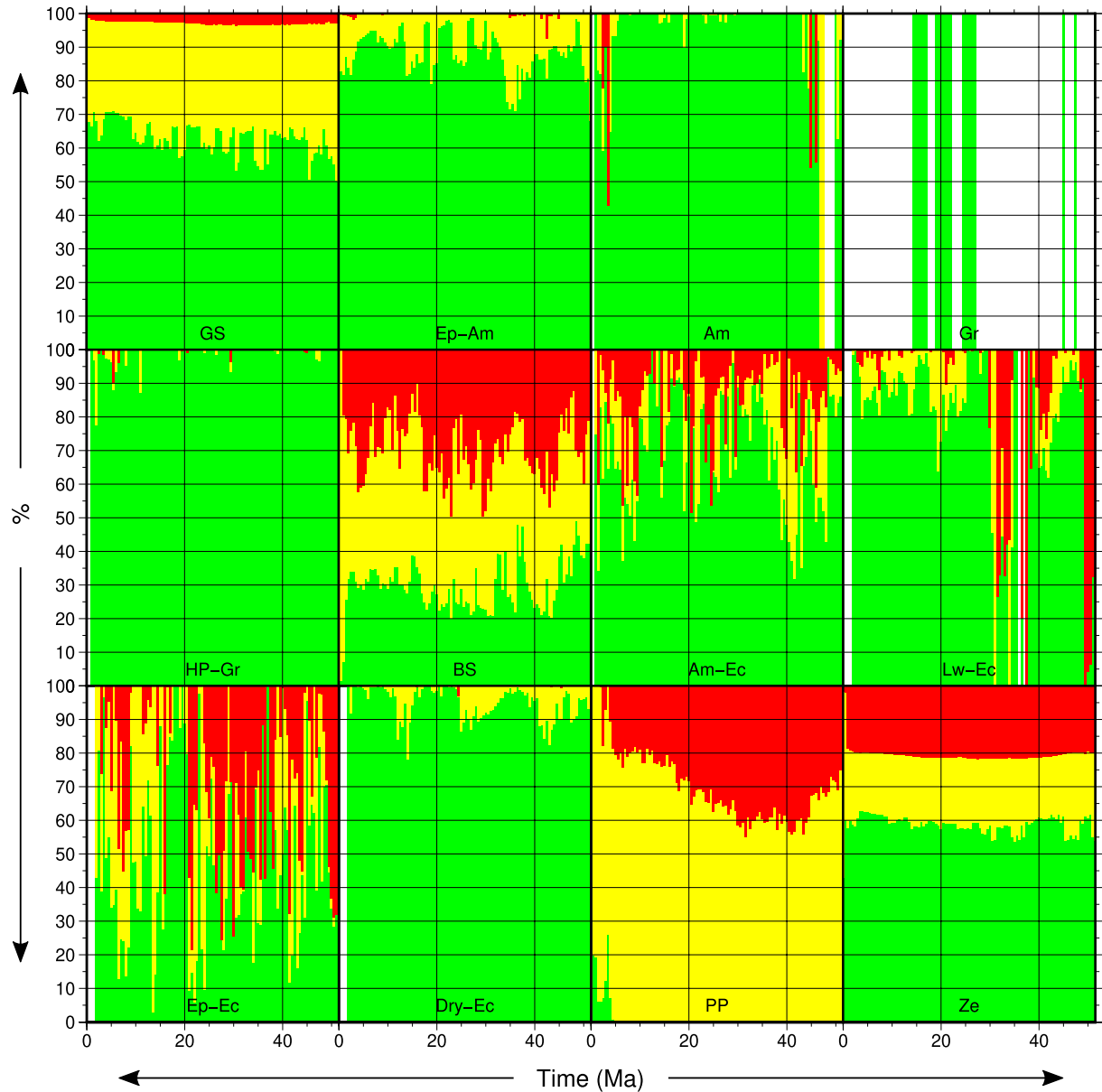


**Figure 8.** Percentages of crustal rocks of model v5 that can record strain rates lower than  $10^{-15} \text{ s}^{-1}$  (green), between  $10^{-15} \text{ s}^{-1}$  and  $10^{-13} \text{ s}^{-1}$  (yellow) and higher than  $10^{-13} \text{ s}^{-1}$  (red) with respect to the total amount of crustal rocks of each metamorphic facies as function of time. White portions indicate the non-existence of the metamorphic facies.

### 3.3.2. Effects of the Subduction Velocity

Maximum strain rates recorded by regions characterized by different metamorphic facies during the evolution show a general increase in models v5 and v8 (Figure 6, panels b and c) with respect to model v3 (Figure 6, panel a). However, this does not correspond to a homogeneously distributed similar increase in the amount of tectonic and mylonitic domains with respect to coronitic domains. Maximum strain rates recorded by the amphibolite and HP-granulite facies regions show a general increase for higher subduction velocities, in particular for model v8, that is characterized by maximum strain rates mainly between  $10^{-13} \text{ s}^{-1}$  and  $10^{-15} \text{ s}^{-1}$ , with some peaks above  $10^{-13} \text{ s}^{-1}$  (Figure 6, panel c). Similarly, the average percentages of crustal rocks that preserve a coronitic texture decrease in models v5 and v8 (green in Figures 8 and 9, respectively), with a correspondent increase in the extent of tectonic and mylonitic domains, up to 60% and 80% in the amphibolite facies and up to 30% and 60% in the HP-granulite facies for models v5 and v8,



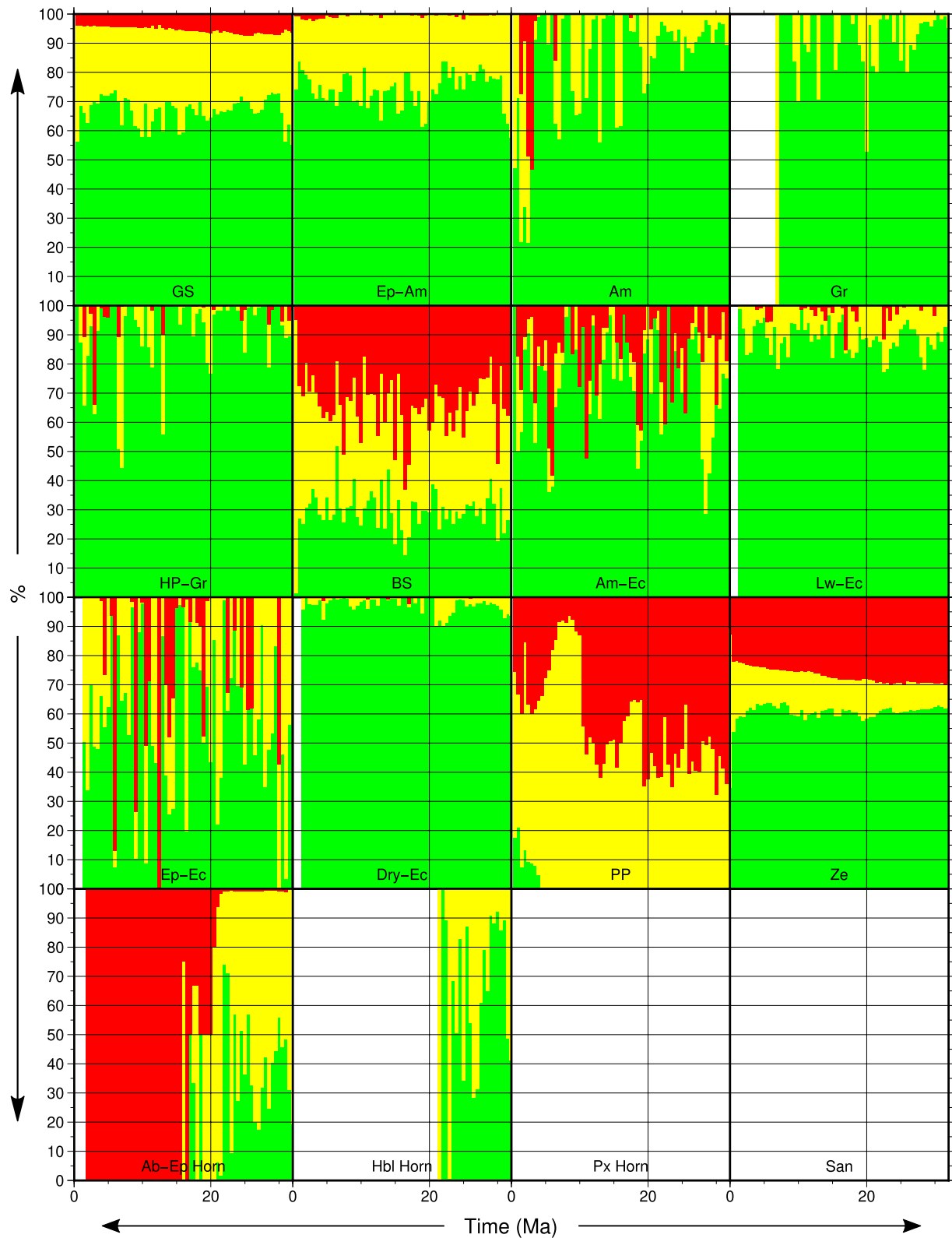


**Figure 9.** Percentages of crustal rocks of model v8 that can record strain rates lower than  $10^{-15} \text{ s}^{-1}$  (green), between  $10^{-15} \text{ s}^{-1}$  and  $10^{-13} \text{ s}^{-1}$  (yellow) and higher than  $10^{-13} \text{ s}^{-1}$  (red) with respect to the total amount of crustal rocks of each metamorphic facies as function of time. White portions indicate the non-existence of the metamorphic facies.

respectively (yellow and red in Figures 8 and 9). However, the most part of crustal rocks still potentially preserves coronitic domains, mostly over 70%. In the same way, the granulite facies shows maximum strain rates lower than  $10^{-15} \text{ s}^{-1}$  in model v5 (Figure 6, panel b), while they are between  $10^{-13} \text{ s}^{-1}$  and  $10^{-15} \text{ s}^{-1}$  in model v8 (Figure 6, panel c), but tectonic fabrics are dominant and occurs from 50% to 100% (green in Figure 9). A general increase of maximum strain rates with the subduction velocity is observed also under the dry-eclogite facies conditions, for which models v5 and v8 show sporadic peaks of maximum strain rates above  $10^{-13} \text{ s}^{-1}$ , more frequent for higher subduction velocities (Figure 6), even if in very limited areas (under 5%; Figures 8 and 9). Differently, there is a decrease of the crustal amount with a dominant tectonic fabric with the increase in the subduction velocity, from a maximum of 25% in model v3 (yellow in Figure 7), to a maximum of 20% in model v5 (yellow in Figure 8) and of 10% in model v8 (yellow in Figure 9).

Under epidote-amphibolite facies conditions the crust shows an increase of maximum strain rates with the increase of the subduction velocity, up to three orders of magnitude, in particular during the second half of the evolution. In fact, maximum strain rates are in the order of  $10^{-14}$ – $10^{-13} \text{ s}^{-1}$  for model v5 and of  $10^{-13}$ – $10^{-12} \text{ s}^{-1}$  for model v8 (Figure 6, panels b and c, respectively). The amount of crustal rocks in which dominant tectonic fabric is expected remains almost constant in models v5 and v8, in particular approximately 20% on average for model v5 (yellow in Figure 8) and 30% on average for model v8 (yellow in Figure 9), while areas potentially able to develop mylonitic fabrics are very limited (less than 5% for models v5 and v8; red in Figures 8 and 9, respectively). Therefore, the largest amount of the crust preserves coronitic fabrics also under epidote-amphibolite facies conditions (green in Figures 8 and 9).

Maximum strain rates under greenschist facies show an increase in model v8, up to approximately  $10^{-12} \text{ s}^{-1}$  (Figure 6, panel c). The amount of crust under greenschist facies that records strain rates compatible with coronitic textures is not influenced by subduction velocity (green in Figures 8 and 9), while there is a widest diffusion of mylonitic fabrics for higher subduction velocities, from 5% in model v5 and 8% in model v8 (red in Figures 8 and 9, respectively). Under zeolite facies conditions there is an increase in the crustal percentage with strain rates above  $10^{-13} \text{ s}^{-1}$  (Figure 6, panels b and c) from 20% in model v5 up to 30% in model v8 (red in Figures 8 and 9, respectively). A similar pattern is observed for the prehnite-pumpellyite facies, which shows an increase of mylonitic fabrics percentage, from 40% in model v5 up to 60% in model v8 (red in Figures 8 and 9).

Blueschist facies rocks show an increase in the maximum strain rates with the increase of subduction velocity, with short peaks of  $10^{-11} \text{ s}^{-1}$  in model v8 (Figure 6, panel c), and a slight increase of the crust percentage with strain rates below  $10^{-15} \text{ s}^{-1}$ , from 30%–40% in model v3 (green in Figure 7) to 20%–30% in models v5 and v8 (green in Figures 8 and 9, respectively), with a concurrent slight increase in regions affected by strain rates above  $10^{-13} \text{ s}^{-1}$ , from 40% in model v3 (red in Figure 7), to 50% in model v5 (red in Figure 8) and 60% in model v8 (red in Figure 9). The amphibole-eclogite facies shows a variable pattern during the evolution in all models, but in general the subduction velocity does not have a clear effect and the majority of the crust can preserve coronitic texture, from 50% to 95% in model v3 (green in Figure 7) and from 30% to 90% in models v5 and v8 (green in Figures 8 and 9, respectively). Although an increase in the maximum strain rates under epidote-eclogite facies for models v5 and v8 (Figure 6, panels b and c), model v8 shows a decrease of mylonitic domains with respect to model v5 (Figures 8 and 9, respectively). Differently from the general trend observed for all the other metamorphic facies, under the lawsonite-eclogite facies there is an increase in the relative amount of crustal rocks that preserve coronitic textures in model v8, which is always above 80% (green in Figure 9).

### 3.4. Spatial Distribution of Deformation Fabrics

Here, we merge the distribution of the metamorphic facies conditions with the coronitic, tectonic and mylonitic domains predicted in different portions of the subduction complex to verify whether under different metamorphic conditions coronitic, tectonic or mylonitic fabrics can develop.

#### 3.4.1. Model v3

The crust of the upper plate is exclusively characterized by low strain rates, such as mainly coronitic texture are expected farther than 50 km from the trench (Figure 10, panels a1–c1). The corresponding low strain rates are predicted under the zeolite, greenschist, epidote-amphibolite and amphibolite facies during the

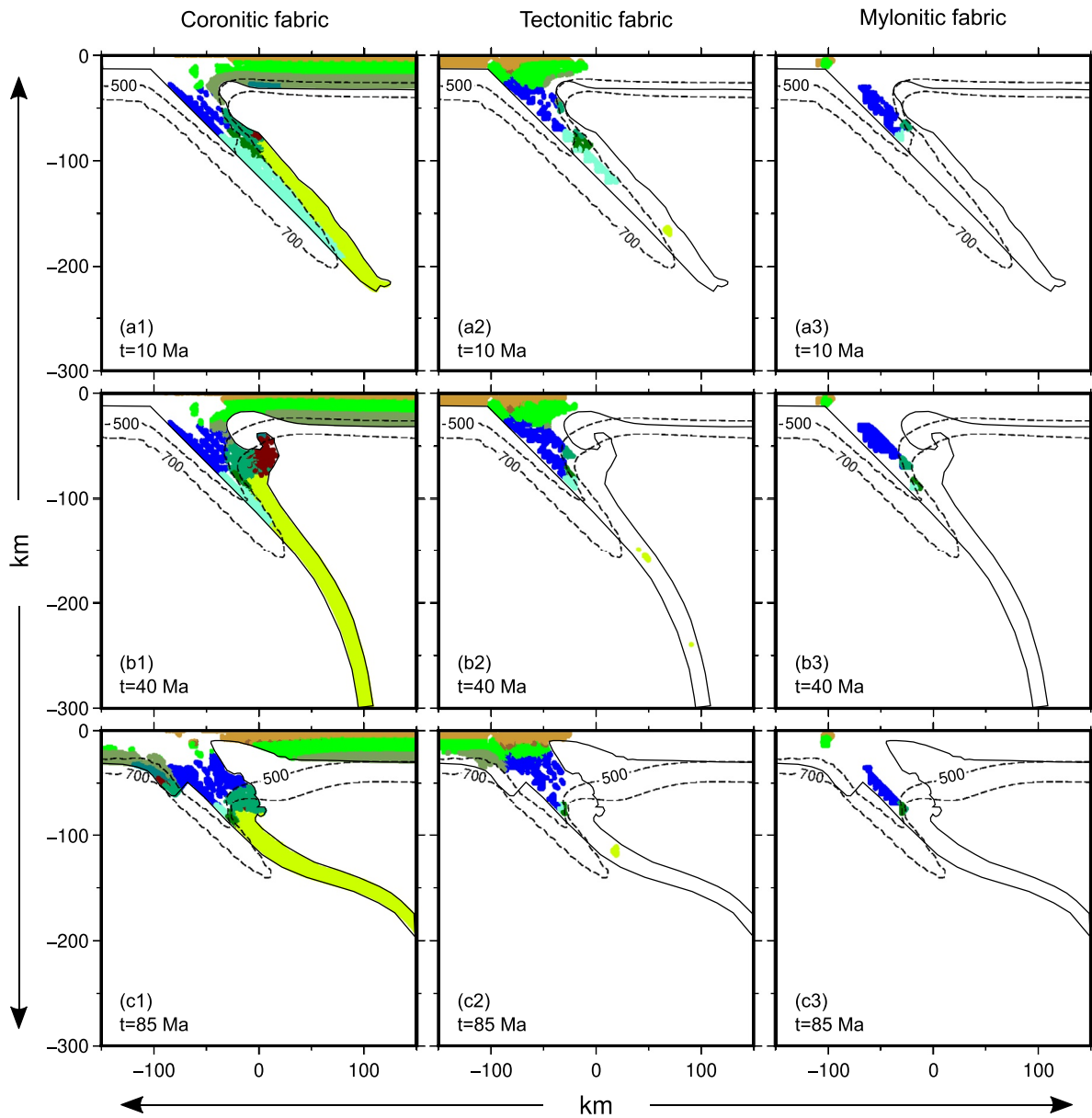


**Figure 10.** Distribution of coronitic (panels a1–c1), tectonic (panels a2–c2) and mylonitic (panels a3–c3) fabrics for each metamorphic facies of model v3 at 10 Ma (panel a), 40 Ma (panel b) and 85 Ma of evolution (panel c). Black continuous lines represent the lower limit of the crust of the upper plate and of the oceanic crust. Black dashed lines represent isotherms 500 and 700°C. Colors of the metamorphic facies as in Figure 2.

whole evolution of the model (Figure 10, panels a1–c1). Strain rates increase toward the trench and a domain with a dominant tectonic fabric can be recognised under zeolite, prehnite-pumpellyite, greenschist, epidote-amphibolite and blueschist facies during the complete evolution (Figure 10, panels a2–c2).

In the mantle wedge area, all fabrics develop contemporaneously. In particular, in the internal portions of the mantle wedge and inside the slab, coronitic, tectonic and mylonitic fabrics occur under all metamorphic facies conditions with a high P/T ratio, such as the blueschist, amphibole-eclogite, epidote-eclogite, dry-eclogite, and lawsonite-eclogite facies (Figure 10, panels a3–c3). Differently, domains undergoing HP-granulite and amphibole-eclogite conditions preserve wide portions of coronitic texture in the external portion of the mantle wedge, which is characterized by temperatures higher than 600°C (Figure 10, panels a1–c1). Deeper than 100 km, the slab is mainly characterized by strain rates compatible with coronitic texture (Figure 10, panels a1–c1), with some domains, up to approximately 170 km depth, in which a tectonic

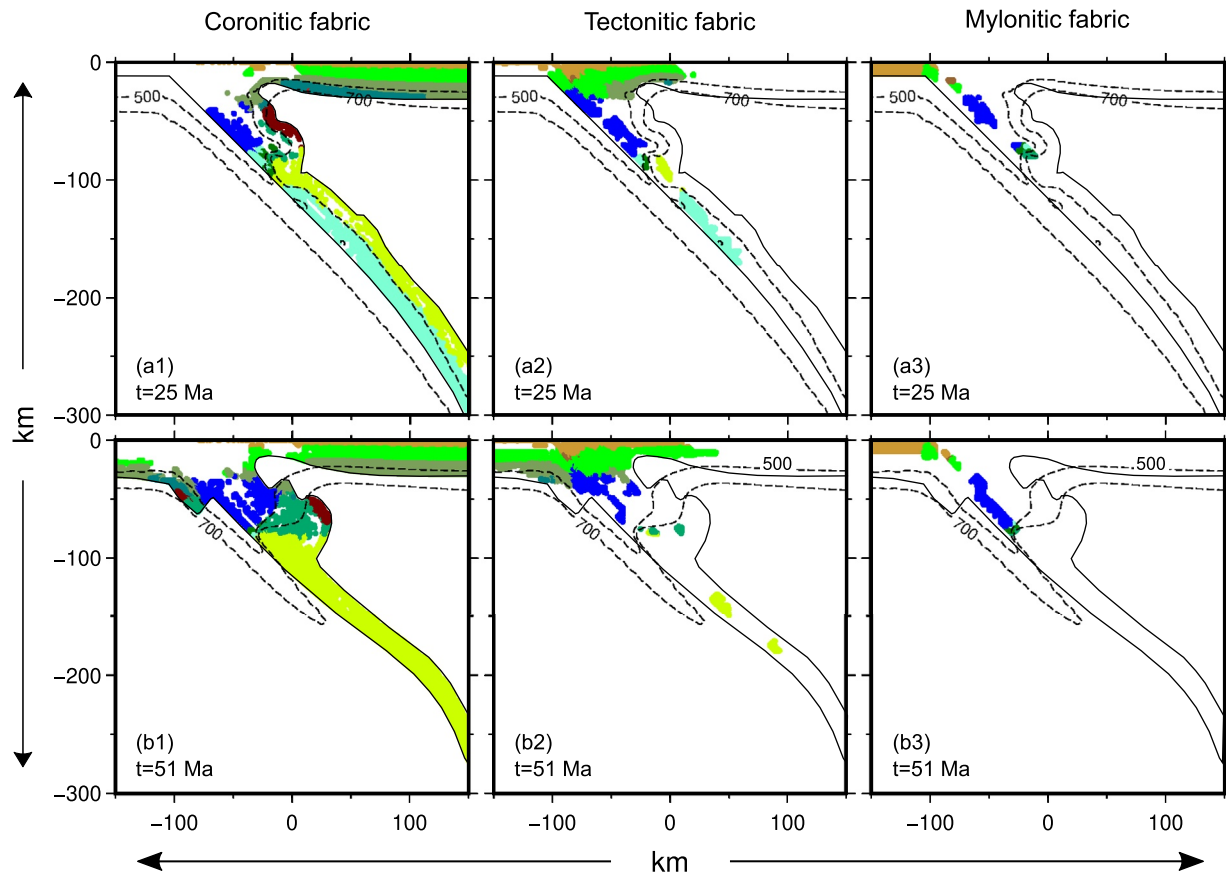


**Figure 11.** Distribution of coronitic (panels a1 and b1), tectonic (panels a2 and b2) and mylonitic (panels a3 and b3) fabrics for each metamorphic facies of model v5 at 25 Ma (panel a) and 51 Ma of evolution (panel b). Black continuous lines represent the lower limit of the crust of the upper plate and of the oceanic crust. Black dashed lines represent isotherms 500 and 700°C. Colors of the metamorphic facies as in Figure 2.

fabric develops (Figure 10, panels a2–c2). Both these fabric domains occur under lawsonite-eclogite and dry-eclogite conditions, in agreement with the different thermal fields predicted during successive convergence stages, as discussed in Section 3.2 (Figure 5). In particular, coronitic and tectonic fabrics are observed in the early evolution, under lawsonite-eclogite conditions, in the internal portion of the slab and under dry-eclogite conditions in the external and warmer part of the slab (Figure 10, panels a1 and a2), while for the late evolution they are observed only under dry-eclogite conditions (Figure 10, panels b1, b2, c1 and c2).

### 3.4.2. Effects of the Subduction Velocity

The increase in the subduction velocity results in a slight increase of strain rates in the upper plate. In particular, domains with dominant tectonic fabrics are observed farther than 100 km from the trench in models v5 (Figure 11, panels a2 and b2) and v8 (Figure 12, panels a2 and b2), while farther away coronitic domains dominate under zeolite, greenschist, epidote-amphibolite and amphibolite facies as in model v3, but also under granulitic conditions in models v5 and v8 (Figure 11, panels a1 and b1 and Figure 12, panels a1 and b1, respectively). Moreover, the subduction velocity increase results in a widening of the region potentially recording a mylonitic fabric close to the trench, under greenschist, zeolite and prehnite-pumpellyite facies conditions (compare Figure 10, panels a3–c3 with Figure 11, panels a3 and b3 and Figure 12, panels a3 and b3).

The increase in the subduction velocity determines an increase of tectonic and mylonitic domains in the central portion of the mantle wedge at the expense of the coronitic domains (Figure 11, panels a3 and b3 and Figure 12, panels a3 and b3), in particular under blueschist conditions. Differently, only coronitic

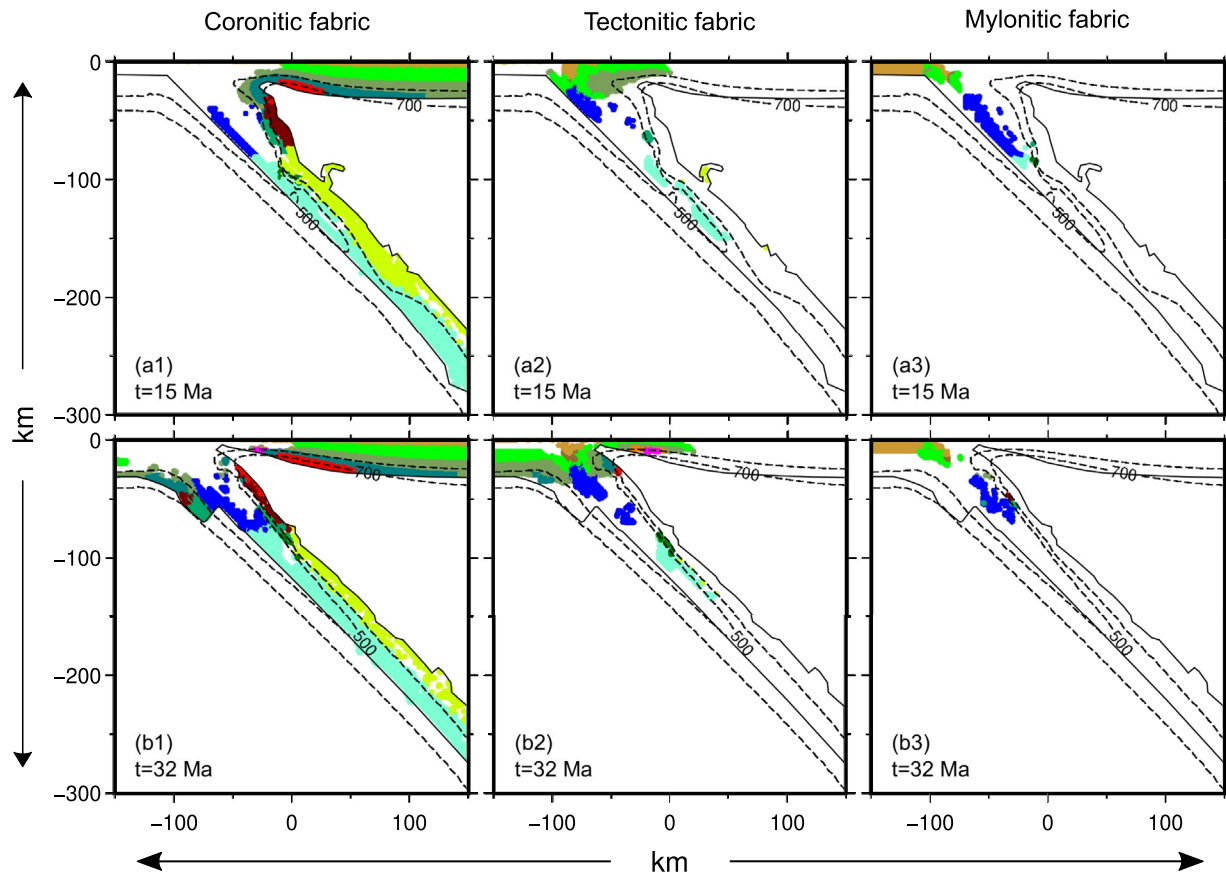


**Figure 12.** Distribution of coronitic (panels a1 and b1), tectonic (panels a2 and b2) and mylonitic (panels a3 and b3) fabrics for each metamorphic facies of model v8 at 15 Ma (panel a) and 32 Ma of evolution (panel b). Black continuous lines represent the lower limit of the crust of the upper plate and of the oceanic crust. Black dashed lines represent isotherms 500 and 700°C. Colors of the metamorphic facies as in Figure 2.

domains are expected in the external portion of the wedge also for higher velocities models (v5 and v8; Figure 11, panels a1 and b1 and Figure 12, panels a1 and b1).

Since the thermal state of the slab deeper than 100 km is largely influenced by the subduction velocity, also the distribution of predicted strain rates under different metamorphic facies varies during the late stages of different models. In particular, in model v5 coronitic domains are observed under lawsonite-eclogite facies in the internal portion of the slab and under dry-eclogite facies in the external portion at half of the evolution (Figure 11, panel a1), while they are expected under dry-eclogite conditions at the end of the evolution (Figure 11, panel b1). In the same way, dominant tectonic domains develop under lawsonite-eclogite or under dry-eclogite conditions at half or at the end of the evolution, respectively (Figure 11, panels a2 and b2). Differently, the colder thermal state predicted by model v8 determines the existence of P-T conditions compatible with the lawsonite-eclogite facies during the whole evolution with the consequent predicted existence of coronitic (Figure 12, panels a1 and a2) and tectonic domains (Figure 12, panels b1 and b2). A general increase of tectonic domains occurs in the deeper portion of the slab with the increase of the subduction velocity in particular during the late evolution (compare Figure 10, panels b2 and c2 with Figure 11, panels a2 and b2 and Figure 12, panels a2 and b2).

#### 4. Discussion

In the context of a 2D numerical model of an ocean-continent subduction process, we tested three different convergence velocities to evaluate their influence on the expected metamorphic facies distribution in the crust and the potentially associated deformation fabrics. The introduction of shear heating, adiabatic heating and latent heat allows the prediction in all models of hotter thermal states with respect to older



geodynamics models, in agreement with the P-T conditions observed in various collisional belts (Penniston-Dorland et al., 2015). The increase of subduction velocity determines lower temperatures inside the slab, related to a progressive intensification of the large-scale mantle flow that causes the advective warming of the subducted slab more effective than the continuous sinking of cold material. Differently, the more intense large-scale mantle flow underneath the overriding plate observed for higher subduction velocities determines higher temperatures at the bottom of the upper plate for model v8 with respect to models v3 and v5.

Moreover, our results show that three domains denoted by contrasted P/T ratios can be recognised within different domains of the same subduction system (Figure 5), on the basis of the distribution of P-T conditions characterizing the different metamorphic facies:

1. A domain identifiable in the upper plate and characterized by intermediate (Barrovian-type metamorphism) P/T ratios and slightly higher than the Abukuma-type metamorphism traditionally interpreted as developed under thermal states characterizing arc regions and plate interiors (black dashed arrows in Figure 13), respectively (Cloos, 1993; England & Richardson, 1977; England & Thompson, 1984; Ernst, 1973; Miyashiro, 1961; Spear, 1993; Thompson, 1981; Thompson & England, 1984). In addition, the increase in the temperature observed during subduction, especially in models v5 and v8, results in the development of epidote-amphibolite facies conditions also in the lower plate (light gray dots in Figure 13, panels c2 and c3) and of amphibolite and granulite facies conditions in the crust of the upper plate (dark gray dots in Figure 13, panels b2, b3, c2 and c3), between 100 and 250 km far from the trench (Figure 5, panels b2, c2 and c3);
2. A domain located in the external part of the mantle wedge with temperatures higher than 600°C and depths shallower than 80 km, which is characterized by intermediate-to-high P/T ratios (comprising part of Barrovian- and of Franciscan-facies series) that has been interpreted as consistent with warm subductions (continuous black arrows in Figure 13). The subduction velocity only influences the extent and the duration of the stability fields of the metamorphic facies (Figure 4) and the increase in temperature in the external portion of the wedge observed in model v8 determines compatibility of the oceanic crust also with HP-granulite, mainly during the first half of the evolution (Figure 5, panels c1 and c2 and light gray dots in Figure 13, panels c1 and c2);
3. A domain located in the internal portion of the mantle wedge (with temperature below 600°C) and along the whole slab below 80 km depth, characterized by high P/T ratios (Franciscan-facies series) interpreted as in tune with cold subductions (dashed-dotted black arrows in Figure 13). In this domain, the oceanic crust of all models attains P-T conditions in the stability fields of blueschist and all types of eclogite facies (Figure 5 and light gray dots in Figure 13) up to 100 km depth, regardless of the subduction velocity. On the contrary, below 100 km depth the subduction velocity has a strong influence during the second part of the evolution, when two metamorphic gradients can be distinguished: one colder, for model v8 and with a predominant compatibility of oceanic crust and crust of the upper plate with lawsonite-eclogite facies conditions (Figure 5, panels c2 and c3 and Figure 13, panels c2 and c3); and one warmer, for models v3 and v5 and with a prevalent compatibility of oceanic crust and crust of the upper plate with dry-eclogite facies conditions (Figure 5, panels a2, a3 and b3 and Figure 13, panels a2, a3 and b3).

The presence of thermally contrasted domains within the same subduction system brings back to the thermal dualism proposed with the concept of paired metamorphic belts (Miyashiro, 1973), more recently revised by Brown (2010). In particular, high subduction velocities allow the attainment of facies typical of the Abukuma-type metamorphism in the crust of the upper plate, as hornblende- and albite-epidote-hornfels facies, contemporaneously with facies typical of the Franciscan-type metamorphism in the internal portion of the mantle wedge, as blueschist and lawsonite-eclogite facies (Figures 5 and 13). However, differently from the original idea of paired metamorphic belts proposed by Miyashiro (1973), our results show the potential development of metamorphic facies characterized by HT and LP-MP also in absence of magmatism, in particular for high subduction velocities (models v5 and v8). The duality of thermal fields predicted by all models regardless of the subduction velocity, even if more emphasized in model v8, is in agreement with the idea that this duality is characteristic of one-sided subductions (Brown, 2010). P-T conditions predicted by the models are also consistent with the contrasted P-T metamorphic conditions and gradients that have been described in the internal zones of some collisional belts. Significantly contrasted P-T metamorphic

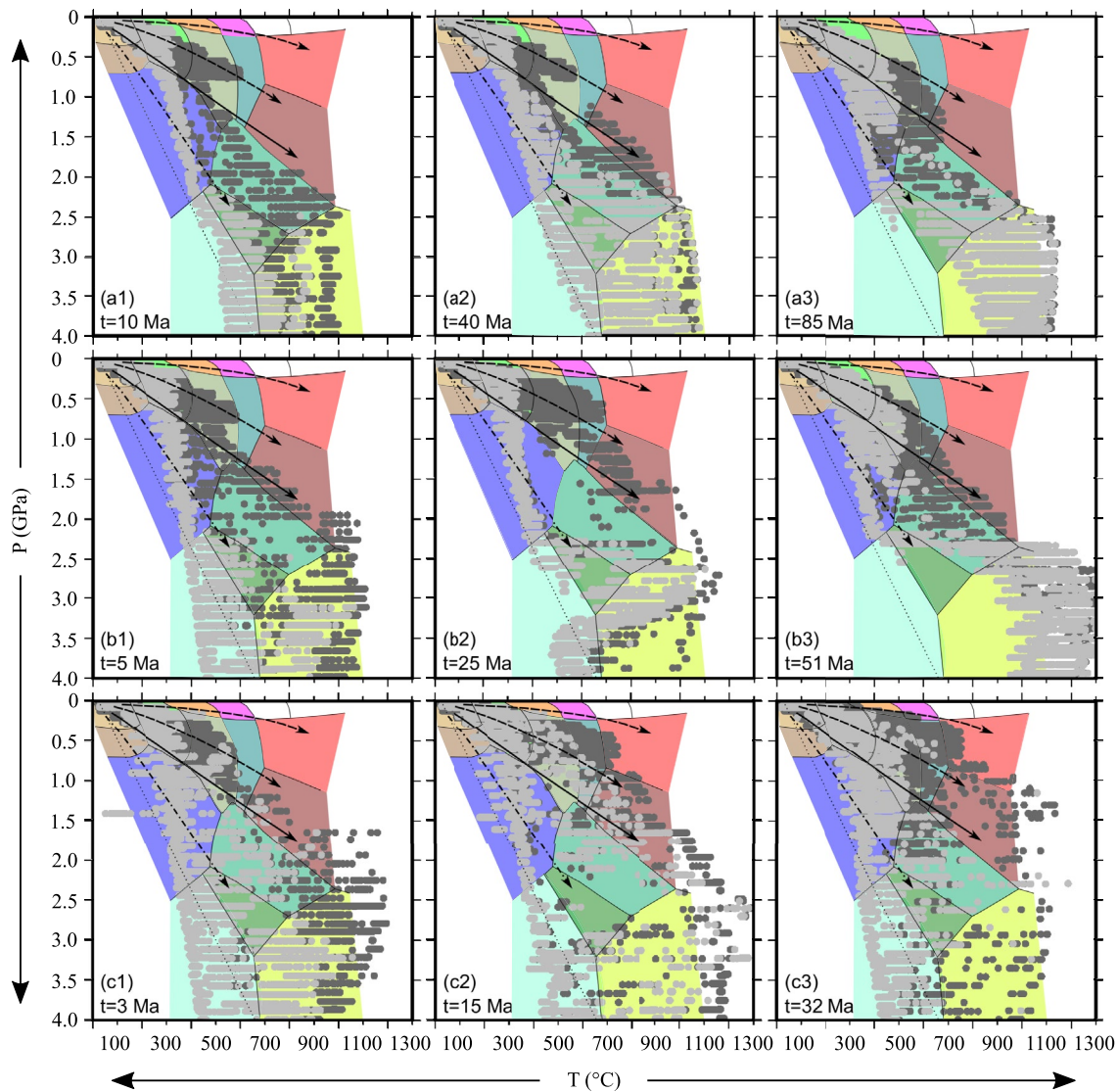


**Figure 13.** Distribution of oceanic crust (light gray dots) and crust of the upper plate (dark gray dots) as function of P-T conditions predicted by models v3, v5, and v8 (panels a, b, and c, respectively) at different times. Black arrows represent geothermal gradients traditionally associated to arc regions and collision zones (dashed arrows), warm subduction complexes (continuous arrow) and cold subduction complexes (dashed-dotted arrow), as presented by Cloos (1993). Black dotted lines represent very low subduction-zone geothermal gradient ( $5^{\circ}\text{C km}^{-1}$ ). Colors of the metamorphic facies are as in Figure 2.

conditions have been recorded during the Variscan subduction, from blueschist, to eclogite and HP-granulite facies (e.g., Ballèvre et al., 2009; Faure et al., 2005; Jouffray et al., 2020; Lardeaux, 2014b; Regorda et al., 2020), as observed in all models (Figure 5).

In addition, our work supports that different metamorphic series and different thermal gradients can co-exist in the same geodynamic setting and can be recorded by the same tectonic unit during its burial and exhumation path, as suggested for rocks belonging to the subduction complex of the Alpine belt (e.g., Roda et al., 2012, 2020; Spalla et al., 1996, 2010). Finally, the crust from upper and lower plates experienced higher P/T ratio conditions for lower convergence velocities. In particular, a large amount of crustal slices lie around the “cold-” and “warm-subduction gradients” in model v3 during the majority of the evolution, showing P-T conditions compatible with amphibolite and HP-granulite facies only at the end of the subduction process (Figure 13, panels a2 and a3). These model predictions are in agreement with the occurrence of metamorphic imprints in the rocks of the subduction complex of the Alps, where low P/T ratios are rarely observed (e.g., Berger & Bousquet, 2008; Bousquet et al., 2008; Lardeaux et al., 2014; Penniston-Dorland

et al., 2015; Roda et al., 2012) in accordance to the low velocity proposed for the Alpine convergence (e.g., Agard et al., 2009; Le Breton et al., 2021; Roda et al., 2010). Differently, both lower and upper plate crustal rocks are affected by higher temperature conditions in faster models since the mid-time evolution. Higher temperatures predicted by the models for higher subduction velocities are in agreement with the conclusions inferred by Penniston-Dorland et al. (2015) comparing P-T data from subduction zones characterized by different convergent velocities. The global distribution of rock slices from upper and lower plates (dark and light gray markers in Figure 13, respectively) indicates that the increment in the convergence velocity allows an increase in the metamorphic gradients that can potentially develop contemporaneously during an oceanic subduction. For highest convergence velocities, metamorphic imprints characterized by low P/T ratios can diffusely coexist with metamorphic imprints distinguished by high P/T ratios and lying along gradients traditionally associated to cold and warm subduction complexes, as described by Cloos (1993) (see dashed-dotted and continuous arrows in Figure 13). Such observation well fits, for example, with the occurrence in the Variscan subduction complex of blueschist- to granulite-facies conditions (e.g., Ballèvre et al., 2009; Faure et al., 2005; Jouffray et al., 2020; Lardeaux, 2014b), in accordance with higher velocities generally proposed for the Variscan convergence (Regorda et al., 2020, and refs. therein).

Our results show that mylonitic units are expected exclusively in the central portion of the mantle wedge (Figures 10–12, panels a3–c3). In fact, in the most internal portion of the mantle wedge the viscosities are relatively high, due to the low temperatures produced by the subducted slab, and the velocity gradients are low since the velocities are strictly controlled by the descending of the slab. Differently, in the external and warmer portion of the mantle wedge the viscosities are higher than those in the internal and colder portions, because the serpentine is no more stable and the rheology is mainly governed by the dry dunite (e.g., Arcay et al., 2005; Gerya & Stöckhert, 2006). Therefore, metamorphic facies that attain a dominant mylonitic fabric are those characterized by temperatures lower than 600°C, where serpentine is stable, and high P/T ratios, such as epidote-eclogite, amphibole-eclogite and, mainly, blueschist facies (Figures 7–9). Pervasive mylonitic domains predicted under epidote-eclogite facies conditions agree with observations of the degree of fabric evolution in the continental crust deeply involved in the Alpine subduction system, where mylonitic fabrics are developed under epidote-eclogite facies in up to the 85% of the rock volume (Zucali et al., 2020). Moreover, the coexistence of mylonitic, tectonic and coronitic, as predicted under blueschist metamorphic facies (Figures 7–9), has been observed in meta-intrusive rocks in the Sesia-Lanzo Zone (Corti et al., 2017) and in the Dent-Blanche Unit (Roda & Zucali, 2011).

The high strain rates (mylonitic fabric) predicted by the models for the HP metamorphic facies occurring within the mantle wedge are consistent with the fabric recorded in the internal domains of the Alps, where highly deformed rocks that have recorded HP metamorphism during their P-T evolution, such as the blueschist and eclogite facies, are often coupled with serpentinized mantle slices (e.g., Malatesta et al., 2012; Roda et al., 2018, 2020). Differently, domains that can better preserve coronitic textures are located in the non-subducted crust of the upper plate and along the slab, where the velocity gradients and strain rates are relatively low, and in the most external portion of the mantle wedge, where the rheology is governed by the strong dry dunite instead of weaker serpentine (Figure 10, panels a1–c1, Figure 11, panels a1 and b1 and Figure 12, panels a1 and b1). In fact, metamorphic facies that result associated with dominant coronitic domains are amphibolite and granulite, which are widespread in the upper plate, HP-granulite, which affects the warmest portion of the mantle wedge, and dry-eclogite, which develops in the colder and deeper portion of the slab (Figure 10, panels a1–c1, Figure 11, panels a1 and b1 and Figure 12, panels a1 and b1). In addition, zeolite, prehnite-pumpellyite, greenschist and epidote-amphibolite metamorphic facies show a decrease in the deformation moving away from the trench (Figure 10, panels a2–c2, Figure 11, panels a2 and b2 and Figure 12, panels a2 and b2), in agreement with observations from the external domains of the Alps (e.g., Handy & Oberhänsli, 2004; Lardeaux et al., 2014), where the Alpine HP metamorphic imprint is missing, and no important pre-collisional ductile structural reworking is reported. In fact, high viscosities and high stresses are predicted in the portion of the upper plate close to the trench, with consequent intermediate strain rates, between  $10^{-15} \text{ s}^{-1}$  and  $10^{-13} \text{ s}^{-1}$ , in agreement with strain rates observed in non-mylonitic deformed rocks (Pfiffner & Ramsay, 1982). Therefore, these low-grade metamorphic facies are characterized by wide dominant tectonic domains associated to wide domains that can better preserve coronitic textures (Figures 7–9). Results predicted by model v3 for the greenschist metamorphic facies are in agreement with estimates of the degree of fabric evolution made on a portion of continental crust of the central Sesia-Lanzo

Zone, where there is a dominance of coronitic domains under greenschist facies conditions (over 80%), while tectonic domains are far less distributed (under 20%) and mylonitic domains have been observed marginally (Zucali et al., 2020).

Although all models show the same relations between metamorphic facies and strain rates, the velocity of subduction determines variations in the relative extent of coronitic, tectonic, and mylonitic domains under some specific metamorphic facies. This is due to different thermal states predicted by the models and, therefore, to the different extent of the metamorphic facies in correspondence of domains characterized by specific strain rates. For example, under greenschist facies conditions an increase in the relative amount of tectonic and mylonitic fabric with the increase in the subduction velocity occurs (Figures 7–9). In fact, in models v5 and v8 the temperatures in the upper plate are higher than in model v3 (see isotherms in Figures 3 and 5), which result in lower viscosities and as a consequence, higher strain rates. Differently, under lawsonite-eclogite conditions a decrease in the relative amount of tectonic and mylonitic fabric occurs for higher subduction velocities (Figures 7–9). This is due to the lower temperatures recorded inside the deep portion of the slab (see isotherms in Figures 3 and 5), with a consequent widening of regions affected by lawsonite-eclogite conditions in a zone characterized by high viscosities and low strain rates (Figure 10, panels a1–c1, Figure 11, panels a1 and b1 and Figure 12, panels a1 and b1).

## 5. Conclusion

By means of 2D thermo-mechanical models, we investigated the evolution of metamorphic facies and associated fabric developments in a convergent system from subduction to the beginning of the continental collision. We found that:

1. The metamorphic facies traditionally associated with continental collisional complexes and characterized by low P/T ratios, such as amphibolite, epidote-amphibolite and granulite, can be also associated with the oceanic subduction, developing at the bottom of the the upper plate crust, in particular for subduction velocities  $\geq 5 \text{ cm yr}^{-1}$ .
2. Three domains characterized by contrasted P/T ratios can be observed in different regions of the convergent margin: (a) a first domain occur in the upper plate and is characterized by low to intermediate P/T ratios; (b) a second domain is located in the external part of the mantle wedge and is characterized by high P/T ratios, corresponding to the gradient traditionally attributed to warm subduction zones; and (c) a third domain corresponds to the internal portion of the mantle wedge or develops along the slab and is characterized by high P/T ratios, traditionally considered characteristic of cold subduction zones.
3. The existence of contrasted metamorphic domains broadens the interpretation of thermal states in converging systems by widening the interpretation of the paired metamorphic belts proposed by Miyashiro (1973), contrasting the narrow perspective that tends to identify each single metamorphic facies series as representative of a specific geodynamic process. In this view, these results can also solve some problematic occurrences of coexisting contrasting metamorphic imprints that characterize adjacent portions of the collisional belts (e.g., the Variscan metamorphic evolution from different areas of the high-pressure tectonic units in the French Massif Central, the Alpine and Himalayan subduction-related orogenic wedges).
4. The varieties of metamorphic gradients that can be potentially recorded during the subduction increases with the convergence velocity. In particular, high convergence velocities allow the existence of granulite and blueschist metamorphic facies at the same time, in agreement with the metamorphic imprints related to the Variscan evolution observed in the French Massif Central and in the Alps. On the contrary, P-T conditions compatible with granulite and amphibole metamorphic facies are hardly reached for low subduction velocities, as observed for the Alpine convergence.
5. Wide domains with dominant coronitic textures can be preserved in the upper plate, farther from the trench for higher subduction velocities, and in the warmest portion of the mantle wedge where metamorphic facies conditions characterized by high temperatures and low-to-medium pressures, such as HP-granulite, granulite and amphibolite facies can be attained.
6. Mylonitic fabrics can be expected mainly in subducted rocks within the serpentinized mantle wedge under LT and HP metamorphic facies, such as blueschist, amphibole-eclogite and epidote-eclogite, and



in the portion of the upper plate close to trench by LT and LP metamorphic facies, such as greenschist, zeolite and prehnite-pumpellyite.

7. Mylonitic fabrics dominate in blueschist and eclogite facies in continental crust generally associated with serpentinized mantle, in agreement with the occurrence of highly deformed tectonic mélange constituted by HP metamorphic rocks and serpentinites described in the internal domains of the Alps.
8. Regions in the upper plate undergoing to greenschist, zeolite, prehnite-pumpellyite and epidote-amphibolite facies conditions, associated with very low strain rates, show similarity with the metamorphic signature observed in the external domains of the Alps where no important pre-collisional ductile deformation is reported and the Alpine HP tectono-metamorphic imprint is lacking.

## Data Availability Statement

Results are presented and developed also in the frame of the MIUR project “Dipartimento di Eccellenza 2017” (Work Package 3, Task 3.4). All figures were created using the Generic Mapping Tool (GMT) plotting software (Wessel & Smith, 1998). All data have been obtained using the numerical code SubMar (Marotta et al., 2006), as described in Regorda et al. (2017) and Marotta et al. (2020).

## Acknowledgments

Alessandro Regorda and Annamaria Marotta have been supported by the ESA funded project Gravitational Seismology ITT AO/1-9101/17/INB. We thank the Editor Whitney Behr and Reviewers Leonardo Casini and Richard Palin for providing useful suggestions.

## References

- Afonso, J. C., & Ranalli, G. (2004). Crustal and mantle strengths in continental lithosphere: Is the jelly sandwich model obsolete? *Tectonophysics*, 394, 221–232. <https://doi.org/10.1016/j.tecto.2004.08.006>
- Agard, P., Yamato, P., Jolivet, L., & Burov, E. (2009). Exhumation of oceanic blueschists and eclogites in subduction zones: Timing and mechanisms. *Earth-Science Reviews*, 92, 53–79. <https://doi.org/10.1016/j.earscirev.2008.11.002>
- Arcay, D., Tric, E., & Doin, M.-P. P. (2005). Numerical simulations of subduction zones. Effect of slab dehydration on the mantle wedge dynamics. *Physics of the Earth and Planetary Interiors*, 149(1–2), 133–153. <https://doi.org/10.1016/j.pepi.2004.08.020>
- Assanelli, M., Luoni, P., Rebay, G., Roda, M., & Spalla, M. I. (2020). Tectono-metamorphic evolution of serpentinites from lanzo valleys subduction complex (Piemonte—Sesia-lanzo zone boundary, Western Italian Alps). *Minerals*, 10(11), 985. <https://doi.org/10.3390/min10110985>
- Ballèvre, M., Bosse, V., Ducassou, C., & Pitra, P. (2009). Palaeozoic history of the Armorican Massif: Models for the tectonic evolution of the suture zones. *Comptes Rendus Geoscience*, 341(2–3), 174–201. <https://doi.org/10.1016/j.crte.2008.11.009>
- Barrow, G. (1912). On the geology of lower dee-side and the southern highland border. *Proceedings of the Geologists' Association*, 23(5), 274. [https://doi.org/10.1016/S0016-7878\(12\)80018-6](https://doi.org/10.1016/S0016-7878(12)80018-6)
- Beach, A. (1976). The interrelations of fluid transport, deformation, geochemistry and heat flow in early proterozoic shear zones in the Lewisian Complex. *Philosophical Transactions of the Royal Society of London Series A*, 280(1298), 569–604. <https://doi.org/10.1098/rsta.1976.0014>
- Berger, A., & Bousquet, R. (2008). Subduction-related metamorphism in the Alps: Review of isotopic ages based on petrology and their geodynamic consequences. *Geological Society, London, Special Publications*, 298, 117–144. <https://doi.org/10.1144/SP298.7>
- Best, M. G., & Christiansen, E. H. (2001). *Igneous petrology*. Blackwell Sci.
- Billen, M. I. (2008). Modeling the dynamics of subducting slabs. *Annual Review of Earth and Planetary Sciences*, 36(1), 325–356. <https://doi.org/10.1146/annurev.earth.36.031207.124129>
- Bohlen, S. R. (1987). Pressure-temperature-time paths and a tectonic model for the evolution of granulites. *The Journal of Geology*, 95(5), 617–632. <https://doi.org/10.1086/629159>
- Bousquet, R., Oberhänsli, R., Goffé, B., Wiederkehr, M., Koller, F., Schmid, S. M., et al. (2008). Metamorphism of metasediments at the scale of an orogen: A key to the Tertiary geodynamic evolution of the Alps. *Geological Society - Special Publications*, 298, 393–411. <https://doi.org/10.1144/SP298.18>
- Brown, M. (2010). Paired metamorphic belts revisited. *Gondwana Research*, 18, 46–59. <https://doi.org/10.1016/j.gr.2009.11.004>
- Carmignani, L., & Kligfield, R. (1990). Crustal extension in the Northern Apennines: The transition from compression to extension in the Alpi Apuane core complex. *Tectonics*, 9(6), 1275–1303. <https://doi.org/10.1029/TC009i006p01275>
- Chopra, P. N., & Peterson, M. S. (1981). The experimental deformation of dunite. *Tectonophysics*, 78, 453–473. [https://doi.org/10.1016/0040-1951\(81\)90024-X](https://doi.org/10.1016/0040-1951(81)90024-X)
- Christensen, U. R., & Yuen, D. A. (1985). Layered convection induced by phase transitions. *Journal of Geophysical Research*, 90(B12), 10291–10300. <https://doi.org/10.1029/jb090ib12p10291>
- Cloos, M. (1982). Flow melanges: Numerical modelling and geological constraints on their origin in the Franciscan subduction complex, California. *The Geological Society of America Bulletin*, 93, 330–345. [https://doi.org/10.1130/0016-7606\(1982\)93<330:fmmmag>2.0.co;2](https://doi.org/10.1130/0016-7606(1982)93<330:fmmmag>2.0.co;2)
- Cloos, M. (1983). Flow mélanges: Numerical modeling and geologic constraints on their origin in the Franciscan subduction complex, California: Reply. *GSA Bulletin*, 94(10), 1243–1244. [https://doi.org/10.1130/0016-7606\(1983\)94<1243:fmmmag>2.0.co;2](https://doi.org/10.1130/0016-7606(1983)94<1243:fmmmag>2.0.co;2)
- Cloos, M. (1993). Lithospheric buoyancy and collisional orogenesis: Subduction of oceanic plateaus, continental margins, island arcs, spreading ridges and seamounts. *The Geological Society of America Bulletin*, 105, 715–737. [https://doi.org/10.1130/0016-7606\(1993\)105<0715:lbacos>2.3.co;2](https://doi.org/10.1130/0016-7606(1993)105<0715:lbacos>2.3.co;2)
- Cloos, M., & Shreve, R. L. (1988a). Subduction-channel model of prism accretion, melange formation, sediment subduction, and subduction erosion at convergent plate margins: 1. Background and description. *Pure and Applied Geophysics*, 128(3/4), 455–500. <https://doi.org/10.1007/bf00874548>
- Cloos, M., & Shreve, R. L. (1988b). Subduction-channel model of prism accretion, melange formation, sediment subduction, and subduction erosion at convergent plate margins: 2. Implication and Discussion. *Pure and Applied Geophysics*, 128(3/4), 501–545. <https://doi.org/10.1007/bf00874549>



- Corti, L., Alberelli, G., Zannoni, D., & Zucali, M. (2017). Analysis of fabric evolution and metamorphic reaction progress at lago della vecchia-valle d'irogna, sesia-lanzo zone, western alps. *Journal of Maps*, 13(2), 521–533. <https://doi.org/10.1080/17445647.2017.1331177>
- Cruciani, C., Carminati, E., & Doglioni, C. (2005). Slab dip vs. lithosphere age: No direct function. *Earth and Planetary Science Letters*, 238, 298–310. <https://doi.org/10.1016/j.epsl.2005.07.025>
- Dai, L., Li, S., Li, Z. H., Somerville, I., Suo, Y., Liu, X., et al. (2018). Dynamics of exhumation and deformation of HP-UHP orogens in double subduction-collision systems: Numerical modeling and implications for the Western Dabie Orogen. *Earth-Science Reviews*, 182(238), 68–84. <https://doi.org/10.1016/j.earscirev.2018.05.005>
- Depine, G. V., Andronicos, C. L., & Phipps-Morgan, J. (2008). Near-isothermal conditions in the middle and lower crust induced by melt migration. *Nature*, 452, 80–83. <https://doi.org/10.1038/nature06689>
- Dubois, J., & Diament, M. (1997). *Géophysique*.
- England, P., & Richardson, S. (1977). The influence of erosion upon the mineral facies of rocks from different metamorphic environments. *Journal of the Geological Society*, 143, 201–213. <https://doi.org/10.1144/gsjgs.134.2.0201>
- England, P., & Thompson, A. (1984). Pressure—Temperature—time paths of regional metamorphism I. Heat transfer during the evolution of regions of thickened continental crust. *Journal of Petrology*, 25(4), 894–928. <https://doi.org/10.1093/petrology/25.4.894>
- Ernst, W. G. (1973). Blueschist metamorphism and P-T regimes in active subduction zones. *Tectonophysics*, 17(3), 255–272. [https://doi.org/10.1016/0040-1951\(73\)90006-1](https://doi.org/10.1016/0040-1951(73)90006-1)
- Ernst, W. G. (1976). Petrologic phase equilibria (Vol. 115, pp. 305–305). Freeman. <https://doi.org/10.1017/S0016756800037201>
- Ernst, W. G. (1977). Tectonics and prograde versus retrograde P-T trajectories of high-pressure metamorphic belts. *Rendiconti Società Italiana di Mineralogia e Petrologia*, 33(1), 191–220.
- Ernst, W. G. (2001). Subduction, ultrahigh-pressure metamorphism, and regurgitation of buoyant crustal slices - Implications for arcs and continental growth. *Physics of the Earth and Planetary Interiors*, 127(1–4), 253–275. [https://doi.org/10.1016/S0031-9201\(01\)00231-X](https://doi.org/10.1016/S0031-9201(01)00231-X)
- Ernst, W. G., & Liou, J. G. (2008). High- and ultrahigh-pressure metamorphism: Past results and future prospects. *American Mineralogist*, 93(11–12), 1771–1786. <https://doi.org/10.2138/am.2008.2940>
- Eskola, P. (1915). On the relation between the chemical and mineralogical composition in the metamorphic rocks of the Orijarvi region. *Bulletin de la Commission Geologique de Finlande*, 44, 109–145.
- Eskola, P. (1920). The mineral facies of rocks. *Norsk Geologisk Tidsskrift*, 6, 143–194.
- Faccenda, M., Gerya, T. V., & Burlini, L. (2009). Deep slab hydration induced by bending-related variations in tectonic pressure. *Nature Geoscience*, 2(11), 790–793. <https://doi.org/10.1038/ngeo656>
- Faccenda, M., & Mancktelow, N. S. (2010). Fluid flow during unbending: Implications for slab hydration, intermediate-depth earthquakes and deep fluid subduction. *Tectonophysics*, 494(1–2), 149–154. <https://doi.org/10.1016/j.tecto.2010.08.002>
- Fagan, T. J., Day, H. W., & Hacker, B. R. (2001). Timing of arc construction and metamorphism in the Slate Creek Complex, northern Sierra Nevada, California. *GSA Bulletin*, 113(8), 1105–1118. [https://doi.org/10.1130/0016-7606\(2001\)113<1105:toacam>2.0.co;2](https://doi.org/10.1130/0016-7606(2001)113<1105:toacam>2.0.co;2)
- Faure, M., Lardeaux, J.-M., & Ledru, P. (2009). A review of the pre-Permian geology of the Variscan French Massif Central. *Comptes Rendus Geoscience*, 341(2–3), 202–213. <https://doi.org/10.1016/j.crte.2008.12.001>
- Faure, M., Mézème, E. B., Cocherie, A., Rossi, P., Chemenda, A., & Boutelier, D. (2008). Devonian geodynamic evolution of the Variscan Belt, insights from the French Massif Central and Massif Armoricain. *Tectonics*, 27(2), 1–19. <https://doi.org/10.1029/2007TC002115>
- Faure, M., Mézème, E. B., Duguet, M., Cartier, C., & Talbot, J. Y. (2005). Paleozoic tectonic evolution of medio-Europa from the example of the French Massif Central and Massif Armoricain. *Journal of the Virtual Explorer*, 19. <https://doi.org/10.3809/jvirtex.2005.00120>
- Favier, A., Lardeaux, J.-M., Legendre, L., Verati, C., Philippon, M., Corsini, M., et al. (2019). Tectono-metamorphic evolution of shallow crustal levels within active volcanic arcs. Insights from the exhumed Basal Complex of Basse-Terre (Guadeloupe, French West Indies). *BSGF - Earth Sciences Bulletin*, 190, 10. <https://doi.org/10.1051/bsgf/2019011>
- Fettes, D. J., & Desmond, J. (2007). *Metamorphic petrology*. Cambridge University Press.
- Fry, N. (1979). Density distribution techniques and strained length methods for determination of finite strains. *Journal of Structural Geology*, 1(3), 221–229. [https://doi.org/10.1016/0191-8141\(79\)90041-5](https://doi.org/10.1016/0191-8141(79)90041-5)
- Gasco, I., Borghi, A., & Gattiglio, M. (2011). P-T Alpine metamorphic evolution of the Monte Rosa nappe along the Piedmont Zone boundary (Gressoney Valley, NW Italy). *Lithos*, 127(1–2), 336–353. <https://doi.org/10.1016/j.lithos.2011.09.007>
- Gerya, T. V. (2010). *Introduction to numerical geodynamic modelling*. Cambridge University Press.
- Gerya, T. V. (2011). Future directions in subduction modeling. *Journal of Geodynamics*, 52(5), 344–378. <https://doi.org/10.1016/j.jog.2011.06.005>
- Gerya, T. V., & Stöckhert, B. (2006). Two-dimensional numerical modeling of tectonic and metamorphic histories at active continental margins. *International Journal of Earth Sciences*, 90(2), 250–274. <https://doi.org/10.1007/s00531-005-0035-9>
- Gerya, T. V., Stöckhert, B., & Perchuk, A. L. (2002). Exhumation of high-pressure metamorphic rocks in a subduction channel: A numerical simulation. *Tectonics*, 21(6), 1–15. <https://doi.org/10.1029/2002TC001406>
- Gerya, T. V., & Yuen, D. A. (2003). Rayleigh–Taylor instabilities from hydration and melting propel ‘cold plumes’ at subduction zones. *Earth and Planetary Science Letters*, 212(1–2), 47–62. [https://doi.org/10.1016/S0012-821X\(03\)00265-6](https://doi.org/10.1016/S0012-821X(03)00265-6)
- Gosso, G., Rebay, G., Roda, M., Spalla, M. I., Tarallo, M., Zannoni, D., & Zucali, M. (2015). Taking advantage of petrostructural heterogeneities in subduction-collisional orogens, and effect on the scale of analysis. *Periodico di Mineralogia*, 84(3B), 779–825. <https://doi.org/10.2451/2015PM0452>
- Guillot, S., Hattori, K., Agard, P., Schwartz, S., & Vidal, O. (2009). Exhumation processes in oceanic and continental subduction contexts: A review. In S. Lallemand, & F. Funicello (Eds.), *Subduction zone dynamics* (pp. 175–204). Springer-Verlag Berlin Heidelberg. <https://doi.org/10.1007/978-3-540-87974-9>
- Guillot, S., Hattori, K. H., De Sigoyer, J., Nägler, T., Auzende, A.-I. L., Sigoyer, D. J., et al. (2001). Evidence of hydration of the mantle wedge and its role in the exhumation of eclogites. *Earth and Planetary Science Letters*, 193(1–2), 115–127. [https://doi.org/10.1016/S0012-821X\(01\)00490-3](https://doi.org/10.1016/S0012-821X(01)00490-3)
- Haenel, R., Rybach, L., & Stegena, L. (1988). *Handbook of terrestrial heat-flow density determination*. Kluwer Academic Publishers.
- Handy, M. R., & Oberhänsli, R. (2004). Explanatory notes to the map: Metamorphic structure of the Alps age map of the metamorphic structure of the Alps - Tectonic interpretation and outstanding problem. *Mitteilungen der Österreichischen Mineralogischen Gesellschaft*, 149, 201–225.
- Handy, M. R., Wissing, S. B., & Streit, L. E. (1999). Frictional–viscous flow in mylonite with varied biminerale composition and its effect on lithospheric strength. *Tectonophysics*, 303(1), 175–191. [https://doi.org/10.1016/S0040-1951\(98\)00251-0](https://doi.org/10.1016/S0040-1951(98)00251-0)

- Hebert, L. B., Antoshechkina, P., Asimow, P., & Gurnis, M. (2009). Emergence of a low-viscosity channel in subduction zones through the coupling of mantle flow and thermodynamics. *Earth and Planetary Science Letters*, 278(3–4), 243–256. <https://doi.org/10.1016/j.epsl.2008.12.013>
- Herwegh, M., Handy, M. R., & Heilbronner, R. (1997). Temperature- and strain-rate-dependent microfabric evolution in monomineralic mylonite: Evidence from in situ deformation of norcamphor. *Tectonophysics*, 280(1–2), 83–106. [https://doi.org/10.1016/S0040-1951\(97\)00139-X](https://doi.org/10.1016/S0040-1951(97)00139-X)
- Hirth, G., & Kohlstedt, D. (2003). Rheology of the upper mantle and the mantle wedge: A view from the experimentalists. *Geophysical Monograph Series*, 138, 83–105. <https://doi.org/10.1029/138GM06>
- Honda, S., & Saito, M. (2003). Small-scale convection under the back arc occurring in the low viscosity wedge. *Earth and Planetary Science Letters*, 216, 703–715. [https://doi.org/10.1016/S0012-821X\(03\)00537-5](https://doi.org/10.1016/S0012-821X(03)00537-5)
- Ismail-Zadeh, A., & Tackley, P. (2010). *Computational methods for geodynamic*. Cambridge University Press.
- Jamieson, R. A., Beaumont, C., Fullsack, P., & Lee, B. (1998). Barrovian regional metamorphism: Where's the heat? *Geological Society of London Special Publications*, 138(1), 23–51. <https://doi.org/10.1144/GSL.SP.1996.138.01.03>
- Ji, W.-Q., Malusà, M. G., Tiepolo, M., Langone, A., Zhao, L., & Wu, F.-Y. (2019). Synchronous periadriatic magmatism in the western and central Alps in the absence of slab breakoff. *Terra Nova*, 31(2), 120–128. <https://doi.org/10.1111/ter.12377>
- Jouffray, F., Spalla, M. I., Lardeaux, J.-M., Filippi, M., Rebay, G., Corsini, M., et al. (2020). Variscan eclogites from the Argentera–Mercantour Massif (External Crystalline Massifs, SW Alps): A dismembered cryptic suture zone. *International Journal of Earth Sciences*, 109, 1273–1294. <https://doi.org/10.1007/s00531-020-01848-2>
- Kirby, S. (1983). Rheology of the lithosphere. *Reviews of Geophysics and Space Physics*, 21(6), 1459–1487. <https://doi.org/10.1029/RG021i006p01458>
- Kornprobst, J. (2002). *Metamorphic rocks and their geodynamic significance. A petrological handbook. Petrology and structural geology series*. Kluwer Academic Publishers.
- Lallemand, S., Heuret, A., & Boutelier, D. (2005). On the relationships between slab dip, back-arc stress, upper plate absolute motion, and crustal nature in subduction zones. *Geochemistry, Geophysics, Geosystems*, 6(9), 1–18. <https://doi.org/10.1029/2005GC000917>
- Lardeaux, J.-M. (2014a). Deciphering orogeny: A metamorphic perspective. Examples from European Alpine and Variscan belts—Part I: Alpine metamorphism in the western Alps. A review. *Bulletin de la Societe Geologique de France*, 185(2), 93–114. <https://doi.org/10.2113/gssgfbull.185.2.93>
- Lardeaux, J.-M. (2014b). Deciphering orogeny: A metamorphic perspective examples from European Alpine and Variscan belts Part II: Variscan metamorphism in the French Massif Central—A review. *Bulletin de la Societe Geologique de France*, 185(5), 281–310. <https://doi.org/10.2113/gssgfbull.185.5.281>
- Lardeaux, J. M., Gosso, G., Kienast, J. R., & Lombardo, B. (1982). Relations entre le métamorphisme et la déformation dans la zone Sézia-Lanzo (Alpes Occidentales) et le problème de l'éclogitisation de la croûte continentale. *Bulletin de la Societe Geologique de France*, 24(4), 793–800. <https://doi.org/10.2113/gssgfbull.s7-xxiv.4.793>
- Lardeaux, J.-M., Schulmann, K., Faure, M., Janousek, V., Lexa, O., Skrzypek, E., et al. (2014). The Moldanubian Zone in the French Massif Central, Vosges/Schwarzwald and Bohemian Massif revisited: Differences and similarities. *Geological Society, London, Special Publications*, 405(1), 7–44. <https://doi.org/10.1144/SP405.14>
- Lardeaux, J. M., & Spalla, M. I. (1990). Tectonic significance of P-T-t paths in metamorphic rocks: Examples from ancient and modern orogenic belts. *Memorie Società Geologica Italiana*, 45, 51–69.
- Le Breton, E., Brune, S., Ustaszewski, K., Zahirovic, S., Seton, M., & Müller, R. D. (2021). Kinematics and extent of the piemont-liguria basin—Implications for subduction processes in the Alps. *Solid Earth*, 12(4), 885–913. <https://doi.org/10.5194/se-12-885-2021>
- Li, Z.-H., Xu, Z., Gerya, T., & Burg, J.-P. (2013). Collision of continental corner from 3-d numerical modeling. *Earth and Planetary Science Letters*, 380, 98–111. <https://doi.org/10.1016/j.epsl.2013.08.034>
- Luoni, P., Rebay, G., Roda, M., Zanoni, D., & Spalla, M. I. (2020). Tectono-metamorphic evolution of UHP Zermatt-Saas serpentinites: A tool for vertical palaeogeographic restoration. *International Geology Review*, 63, 1–26. <https://doi.org/10.1080/00206814.2020.1758967>
- Magni, V., Bouilhol, P., & van Hunen, J. (2014). Deep water recycling through time. *Geochemistry, Geophysics, Geosystems*, 15, 4203–4216. <https://doi.org/10.1002/2014GC005525>
- Malatesta, C., Gerya, T., Scambelluri, M., Federico, L., Crispini, L., & Capponi, G. (2012). Intraoceanic subduction of “heterogeneous” oceanic lithosphere in narrow basins: 2D numerical modeling. *Lithos*, 140–141(0), 234–251. <https://doi.org/10.1016/j.lithos.2012.01.003>
- Manzotti, P., Zucali, M., Balleve, M., Robyr, M., & Engi, M. (2014). Geometry and kinematics of the Roisan-Cignana Shear Zone and the orogenic evolution of the Dent Blanche Tectonic System (Western Alps). *Swiss Journal of Geosciences*, 107(1), 23–47. <https://doi.org/10.1007/s00015-014-0157-9>
- Marotta, A. M., Restelli, F., Bollino, A., Regorda, A., & Sabadini, R. (2020). The static and time-dependent signature of ocean-continent and ocean-ocean subduction: The case studies of Sumatra and Mariana complexes. *Geophysical Journal International*, 221(2), 788–825. <https://doi.org/10.1093/gji/ggaa029>
- Marotta, A. M., Roda, M., Conte, K., & Spalla, M. I. (2016). Thermo-mechanical numerical model of the transition from continental rifting to oceanic spreading: The case study of the Alpine Tethys. *Geological Magazine*, 155(2), 250–279. <https://doi.org/10.1017/S0016756816000856>
- Marotta, A. M., & Spalla, M. I. (2007). Permian-Triassic high thermal regime in the Alps: Result of late Variscan collapse or continental rifting? Validation by numerical modeling. *Tectonics*, 26, 1–27. <https://doi.org/10.1029/2006TC002047>
- Marotta, A. M., Spelta, E., & Rizzetto, C. (2006). Gravity signature of crustal subduction inferred from numerical modelling. *Geophysical Journal International*, 166, 923–938. <https://doi.org/10.1111/j.1365-246X.2006.03058.x>
- Meda, M., Marotta, A. M., & Spalla, M. I. (2010). The role of mantle hydration into the continental crust recycling in the wedge region. *Geological Society, London, Special Publications*, 332, 149–172. <https://doi.org/10.1144/sp332.10>
- Mehl, L., & Hirth, G. (2008). Plagioclase preferred orientation in layered mylonites: Evaluation of flow laws for the lower crust. *Journal of Geophysical Research*, 113(5), 1–19. <https://doi.org/10.1029/2007JB005075>
- Menant, A., Sternai, P., Jolivet, L., Guillou-Frottier, L., & Gerya, T. (2016). 3d numerical modeling of mantle flow, crustal dynamics and magma genesis associated with slab roll-back and tearing: The eastern mediterranean case. *Earth and Planetary Science Letters*, 442, 93–107. <https://doi.org/10.1016/j.epsl.2016.03.002>
- Mevel, C., Caby, R., & Kienast, J.-R. (1978). Amphibolite facies conditions in the oceanic crust: Example of amphibolitized flaser-gabbro and amphibolites from the Chenaillet ophiolite massif (Hautes Alpes, France). *Earth and Planetary Science Letters*, 39(1), 98–108. [https://doi.org/10.1016/0012-821X\(78\)90146-2](https://doi.org/10.1016/0012-821X(78)90146-2)
- Miyashiro, A. (1961). Evolution of metamorphic belts. *Journal of Petrology*, 2, 277–311. <https://doi.org/10.1093/petrology/2.3.277>

- Miyashiro, A. (1973). Paired and unpaired metamorphic belts. *Tectonophysics*, 17, 241–254. [https://doi.org/10.1016/0040-1951\(73\)90005-x](https://doi.org/10.1016/0040-1951(73)90005-x)
- Norris, R. J., & Cooper, A. F. (2003). Very high strains recorded in mylonites along the Alpine Fault, New Zealand: Implications for the deep structure of plate boundary faults. *Journal of Structural Geology*, 25(12), 2141–2157. [https://doi.org/10.1016/S0191-8141\(03\)00045-2](https://doi.org/10.1016/S0191-8141(03)00045-2)
- Oberhänsli, R., & Goffé, B. (2004). Explanatory notes to the map: Metamorphic structure of the Alps Introduction. *Mitteilungen der Österreichischen Mineralogischen Gesellschaft*, 149, 115–123.
- Okudaira, T., & Shigematsu, N. (2012). Estimates of stress and strain rate in mylonites based on the boundary between the fields of grain-size sensitive and insensitive creep. *Journal of Geophysical Research*, 117(3), 1–15. <https://doi.org/10.1029/2011JB008799>
- Oxburgh, E. R., & Turcotte, D. L. (1970). Thermal Structure of Island Arcs. *GSA Bulletin*, 81(6), 1665–1688. [https://doi.org/10.1130/0016-7606\(1970\)81\[1665:tsoia\]2.0.co;2](https://doi.org/10.1130/0016-7606(1970)81[1665:tsoia]2.0.co;2)
- Oxburgh, E. R., & Turcotte, D. L. (1971). Origin of paired metamorphic belts and crustal dilation in island arc regions. *Journal of Geophysical Research*, 76(5), 1315–1327. <https://doi.org/10.1029/JB076i005p01315>
- Passchier, C. W., & Trouw, R. A. J. (2005). *Microtectonics*. Springer.
- Peacock, S. M. (1989). Metamorphic pressure-temperature-time paths. In F. S. Spear, & S. M. Peacock (Eds.), American Geophysical Union. <https://doi.org/10.1029/SC007>
- Peacock, S. M. (1990a). Fluid processes in subduction zones. *Science*, 248, 329–337. <https://doi.org/10.1126/science.248.4953.329>
- Peacock, S. M. (1990b). Numerical simulation of metamorphic pressure-temperature-time paths and fluid production in subducting slabs. *Tectonics*, 9(5), 1197–1211. <https://doi.org/10.1029/TC009i005p01197>
- Penniston-Dorland, S. C., Kohn, M. J., & Manning, C. E. (2015). The global range of subduction zone thermal structures from exhumed blueschists and eclogites: Rocks are hotter than models. *Earth and Planetary Science Letters*, 428, 243–254. <https://doi.org/10.1016/j.epsl.2015.07.031>
- Pfiffner, O. A., & Ramsay, J. G. (1982). Conventional strain. *Journal of Geophysical Research*, 87(B1), 311–321. <https://doi.org/10.1029/jb087ib01p00311>
- Pognante, U., Rösli, U., & Toscani, L. (1985). Petrology of ultramafic and mafic rocks from the Lanzo peridotite body (Western Alps). *Lithos*, 18, 201–214. [https://doi.org/10.1016/0024-4937\(85\)90025-8](https://doi.org/10.1016/0024-4937(85)90025-8)
- Prior, D. J., Knipe, R. J., & Handy, M. R. (1990). Estimates of the rates of microstructural changes in mylonites. *Geological Society - Special Publications*, 54(54), 309–319. <https://doi.org/10.1144/GSL.SP.1990.054.01.27>
- Quinquis, M. E., & Buiter, S. J. (2014). Testing the effects of basic numerical implementations of water migration on models of subduction dynamics. *Solid Earth*, 5(1), 537–555. <https://doi.org/10.5194/se-5-537-2014>
- Ramsay, J. G., & Graham, R. H. (1970). Strain variation in shear belts. *Canadian Journal of Earth Sciences*, 7(3), 786–813. <https://doi.org/10.1139/e70-078>
- Ranalli, G., & Murphy, D. C. D. (1987). Rheological stratification of the lithosphere. *Tectonophysics*, 132(4), 281–295. [https://doi.org/10.1016/0040-1951\(87\)90348-9](https://doi.org/10.1016/0040-1951(87)90348-9)
- Regorda, A., Lardeaux, J. M., Roda, M., Marotta, A. M., & Spalla, M. I. (2020). How many subductions in the Variscan orogeny? Insights from numerical models. *Geoscience Frontiers*, 11(3), 1025–1052. <https://doi.org/10.1016/j.gsf.2019.10.005>
- Regorda, A., Roda, M., Marotta, A. M., & Spalla, M. I. (2017). 2-D numerical study of hydrated wedge dynamics from subduction to post-collisional phases. *Geophysical Journal International*, 211(2), 974–1000. <https://doi.org/10.1093/gji/ggx336>
- Roda, M., Marotta, A. M., & Spalla, M. I. (2010). Numerical simulations of an ocean-continent convergent system: Influence of subduction geometry and mantle wedge hydration on crustal recycling. *Geochemistry, Geophysics, Geosystems*, 11(5), 1–21. <https://doi.org/10.1029/2009GC003015>
- Roda, M., Marotta, A. M., & Spalla, M. I. (2011). The effects of the overriding plate thermal state on the slab dip in an ocean-continent subduction system. *Compte Rendu Academie des Sciences Paris*, 343(5), 323–330. <https://doi.org/10.1016/j.crte.2011.01.005>
- Roda, M., Spalla, M. I., & Marotta, A. M. (2012). Integration of natural data within a numerical model of ablative subduction: A possible interpretation for the Alpine dynamics of the Austroalpine crust. *Journal of Metamorphic Geology*, 30(9), 973–996. <https://doi.org/10.1111/jmg.12000>
- Roda, M., & Zucali, M. (2011). Tectono-metamorphic map of the Mont Morion Permian metaintrusives (Mont Morion—Mont Collon—Matterhorn Complex, Dent Blanche Unit), Valpelline—Western Italian Alps. *Journal of Maps*, 7, 519–535. <https://doi.org/10.4113/jom.2011.1194>
- Roda, M., Zucali, M., Corti, L., Visalli, R., Ortolano, G., & Spalla, M. I. (2021). Blueschist mylonitic zones accommodating syn-subduction exhumation of deeply buried continental crust: The example of the Rocca Canavese Thrust Sheets Unit (Sesia-Lanzo Zone, Italian Western Alps). *Swiss Journal of Geosciences*, 114(6), 1–33. <https://doi.org/10.1186/s00015-021-00385-7>
- Roda, M., Zucali, M., Li, Z. X., Spalla, M. I., & Yao, W. (2018). Pre-Alpine contrasting tectono-metamorphic evolutions within the Southern Steep Belt, Central Alps. *Lithos*, 310–311, 31–49. <https://doi.org/10.1016/j.lithos.2018.03.025>
- Roda, M., Zucali, M., Regorda, A., & Spalla, M. I. (2020). Formation and evolution of a subduction-related melange: The example of the Rocca Canavese Thrust Sheets (Western Alps). *Bulletin of the Geological Society of America*, 132(3–4), 884–896. <https://doi.org/10.1130/B35213.1>
- Rothstein, D. A., & Manning, C. E. (2003). Geothermal gradients in continental magmatic arcs: Constraints from the eastern peninsular ranges-escarpment, Baja California, México. *Special Papers - Geological Society of America*, 337–354. <https://doi.org/10.1130/0-8137-2374-4.337>
- Rupke, L. H., Morgan, J. P., Hort, M., Connolly, J. A. D., Phipps Morgan, J., Hort, M., et al. (2004). Serpentine and the subduction zone water cycle. *Earth and Planetary Science Letters*, 223(1–2), 17–34. <https://doi.org/10.1016/j.epsl.2004.04.018>
- Sandiford, M., & Powell, R. (1991). Some remarks on high-temperature—Low-pressure metamorphism in convergent orogens. *Journal of Metamorphic Geology*, 9(3), 333–340. <https://doi.org/10.1111/j.1525-1314.1991.tb00527.x>
- Schliffke, N., van Hunen, J., Magni, V., & Allen, M. B. (2019). The role of crustal buoyancy in the generation and emplacement of magmatism during continental collision. *Geochemistry, Geophysics, Geosystems*, 20(11), 4693–4709. <https://doi.org/10.1029/2019GC008590>
- Schmidt, M. W., & Poli, S. (1998). Experimentally based water budgets for dehydrating slabs and consequences for arc magma generation. *Earth and Planetary Science Letters*, 163, 361–379. [https://doi.org/10.1016/S0012-821X\(98\)00142-3](https://doi.org/10.1016/S0012-821X(98)00142-3)
- Schwartz, S., Allemand, P., & Guillot, S. (2001). Numerical model of the effect of serpentinites on the exhumation of eclogitic rocks: Insights from the Monviso ophiolitic massif (Western Alps). *Tectonophysics*, 342(1–2), 193–206. [https://doi.org/10.1016/S0040-1951\(01\)00162-7](https://doi.org/10.1016/S0040-1951(01)00162-7)
- Sizova, E., Hauzenberger, C., Fritz, H., Faryad, S. W., & Gerya, T. (2019). Late orogenic heating of (ultra)high pressure rocks: Slab rollback vs. slab breakoff. *Geosciences*, 9(12), 499. <https://doi.org/10.3390/geosciences9120499>
- Spalla, M. I., Gosso, G., Marotta, A. M., Zucali, M., & Salvi, F. (2010). Analysis of natural tectonic systems coupled with numerical modelling of the polycyclic continental lithosphere of the Alps. *International Geology Review*, 52(10–12), 1268–1302. <https://doi.org/10.1080/00206814.2010.482737>

- Spalla, M. I., Lardeaux, J.-M., Dal Piaz, G. V., Gosso, G., & Messiga, B. (1996). Tectonic significance of alpine eclogites. *Journal of Geodynamics*, 21(3), 257–285. [https://doi.org/10.1016/0264-3707\(95\)00033-X](https://doi.org/10.1016/0264-3707(95)00033-X)
- Spalla, M. I., & Zucali, M. (2004). Deformation vs. metamorphic re-equilibration heterogeneities in polymetamorphic rocks: A key to infer quality P-T-d-t path. *Rivista Italiana di Mineralogia e Petrologia*, 73, 249.
- Spear, F. S. (1993). *Metamorphic phase equilibria and Pressure-Temperature-time paths*. Monographs - Mineralogical Society of America.
- Spry, A. (1969). *Metamorphic textures*. Pergamon Press.
- Stern, R. J., & Gerya, T. (2018). Subduction initiation in nature and models: A review. *Tectonophysics*, 746(October), 173–198. <https://doi.org/10.1016/j.tecto.2017.10.014>
- Tamblyn, R., Hand, M., Morrissey, L., Zack, T., Phillips, G., & Och, D. (2020). Resubduction of lawsonite eclogite within a serpentinite-filled subduction channel. *Contributions to Mineralogy and Petrology*, 175(8), 74. <https://doi.org/10.1007/s00410-020-01712-1>
- Teall, J. J. H. (1885). The metamorphosis of dolerite into hornblende-schist. *Quarterly Journal of the Geological Society*, 41(1–4), 133–145. <https://doi.org/10.1144/GSL.JGS.1885.041.01-04.19>
- Thieulot, C. (2014). ELEFANT: A user-friendly multipurpose geodynamics code. *Solid Earth Discussions*, 6(2), 1949–2096. <https://doi.org/10.5194/sed-6-1949-2014>
- Thompson, A. B. (1981). The pressure-temperature (P, T) plane viewed by geophysicists and petrologists. *Terra Cognita*, 1, 11–20. [https://doi.org/10.1016/0377-0273\(81\)90072-x](https://doi.org/10.1016/0377-0273(81)90072-x)
- Thompson, A. B., & England, P. C. (1984). Pressure–temperature–time paths of regional metamorphism II. Their inference and interpretation using mineral assemblages in metamorphic rocks. *Journal of Petrology*, 25(4), 929–955. <https://doi.org/10.1093/ptrology/25.4.929>
- Toksöz, M., & Bird, P. (1977). Modelling of temperatures in continental convergence zones. *Tectonophysics*, 41(1), 181–193. [https://doi.org/10.1016/0040-1951\(77\)90189-5](https://doi.org/10.1016/0040-1951(77)90189-5)
- Tosi, N., Stein, C., Noack, L., Hüttig, C., Maierová, P., Samuel, H., et al. (2015). A community benchmark for viscoplastic thermal convection in a 2-D square box. *Geochemistry, Geophysics, Geosystems*, 16, 2175–2196. <https://doi.org/10.1002/2015GC005807>
- Turcotte, D. L., & Schubert, G. (2002). *Geodynamics* (2nd ed.). Cambridge University Press.
- Turner, F. J. (1981). *Metamorphic petrology*. McGraw-Hill.
- van Hunen, J., & Allen, M. B. (2011). Continental collision and slab break-off: A comparison of 3-D numerical models with observations. *Earth and Planetary Science Letters*, 302(1–2), 27–37. <https://doi.org/10.1016/j.epsl.2010.11.035>
- van Keken, P. E., Currie, C., King, S. D., Behn, M. D., Cagnioncle, A., He, J., et al. (2008). A community benchmark for subduction zone modeling. *Physics of the Earth and Planetary Interiors*, 171(1–4), 187–197. <https://doi.org/10.1016/j.pepi.2008.04.015>
- van Keken, P. E., King, S. D., Schmeling, H., Christensen, U. R., Neumeister, D., & Doin, M.-P. (1997). A comparison of methods for the modeling of thermochemical convection. *Journal of Geophysical Research*, 102(B10), 22477–22495. <https://doi.org/10.1029/97JB01353>
- Vanderhaeghe, O. (2012). The thermal–mechanical evolution of crustal orogenic belts at convergent plate boundaries: A reappraisal of the orogenic cycle. *Journal of Geodynamics*, 56–57, 124–145. <https://doi.org/10.1016/j.jog.2011.10.004>
- Verati, C., Lardeaux, J.-M., Favier, A., Corsini, M., Philippon, M., & Legendre, L. (2018). Arc-related metamorphism in the Guadeloupe archipelago (Lesser Antilles active island arc): First report and consequences. *Lithos*, 320–321, 592–598. <https://doi.org/10.1016/j.lithos.2018.08.005>
- Wang, Y., Zhang, L. F., Li, Z. H., Li, Q. Y., & Bader, T. (2019). The exhumation of subducted oceanic-derived eclogites: Insights from phase equilibrium and thermomechanical modeling. *Tectonics*, 38(1), 34–1797. <https://doi.org/10.1029/2018TC005349>
- Warren, C. J., Beaumont, C., & Jamieson, R. A. (2008). Modelling tectonic styles and ultra-high pressure (UHP) rock exhumation during the transition from oceanic subduction to continental collision. *Earth and Planetary Science Letters*, 267, 129–145. <https://doi.org/10.1016/j.epsl.2007.11.025>
- Wessel, P., & Smith, W. H. F. (1998). New, improved version of generic mapping tools released. *Eos, Transactions American Geophysical Union*, 79(47), 579–579. <https://doi.org/10.1029/98EO00426>
- White, S. (1979). Grain and sub-grain size variations across a mylonite zone. *Contributions to Mineralogy and Petrology*, 70(2), 193–202. <https://doi.org/10.1007/BF00374448>
- Yamato, P., Agard, P., Burov, E., Le Pourhiet, L., Jolivet, L., Tiberi, C., et al. (2007). Burial and exhumation in a subduction wedge: Mutual constraints from thermomechanical modeling and natural P-T-t data (Schistes Lustrés, western Alps). *Journal of Geophysical Research: Solid Earth*, 112(7), 1–28. <https://doi.org/10.1029/2006JB004441>
- Yardley, B. (1989). *An introduction to metamorphic petrology*. Longman Scientific & Technical.
- Yardley, B., & Warren, C. (2020). *An introduction to metamorphic petrology*.
- Zucali, M., Corti, L., Delleani, F., Zannoni, D., & Spalla, M. I. (2020). 3D reconstruction of fabric and metamorphic domains in a slice of continental crust involved in the Alpine subduction system: The example of Mt. Mucrone (Sesia–Lanzo Zone, Western Alps). *International Journal of Earth Sciences*, 109(4), 1337–1354. <https://doi.org/10.1007/s00531-019-01807-6>